

This is to certify that the

thesis entitled

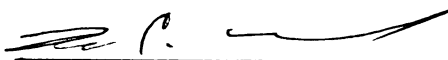
A CHARACTERIZATION AND APPLICATIONS OF HIGH
IMPEDANCE GROUND PLANES WITH CONFORMAL ANTENNAS

presented by

BENJAMIN RUSSELL WILMHOFF

has been accepted towards fulfillment
of the requirements for

MS degree in ELECTRICAL ENGINEERING



Major professor

Date 7/31/02

LIBRARY
Michigan State
University

PLACE IN RETURN BOX to remove this checkout from your record.
TO AVOID FINES return on or before date due.
MAY BE RECALLED with earlier due date if requested.

DATE DUE	DATE DUE	DATE DUE

**A CHARACTERIZATION AND APPLICATIONS OF HIGH IMPEDANCE
GROUND PLANES WITH CONFORMAL ANTENNAS**

By

Benjamin Russell Wilmhoff

A THESIS

**Submitted to
Michigan State University
in partial fulfillment of the requirements
for the degree of**

MASTER OF SCIENCE

Department of Electrical Engineering

2002

UMI Number: 1410744

UMI[®]

UMI Microform 1410744

Copyright 2002 by ProQuest Information and Learning Company.
All rights reserved. This microform edition is protected against
unauthorized copying under Title 17, United States Code.

ProQuest Information and Learning Company
300 North Zeeb Road
P.O. Box 1346
Ann Arbor, MI 48106-1346

ABSTRACT

A CHARACTERIZATION AND APPLICATIONS OF HIGH IMPEDANCE GROUND PLANES WITH CONFORMAL ANTENNAS

By

Benjamin Russell Wilmhoff

Current conformal antenna designs often incorporate features which protect surrounding devices from unwanted radiation from the antenna. These antennas include patch antennas and printed dipoles, amongst others. These features, in the form of larger ground planes or absorber-loaded quarter-wave cavities, often are detrimental to the performance of the antenna itself. A relatively new advance in electromagnetic engineering, physics and optics, called the photonic band-gap (PBG) structure and the high impedance ground plane (HIGP) have proven useful in alleviating these effects.

This thesis first highlights the operation of HIGPs and provides computational analysis, using the Finite Element Method (FEM), of a hybrid HIGP/conformal antenna design. Secondly, a novel four-layer design concept for HIGP/antenna structures is presented. This concept uses electric-type or real-source antennas, such as a dipole, placed parallel in close proximity to the HIGP structure separated by a thin layer of low-dielectric material. This design concept helps to better match the antenna by eliminating the phase-reversed reflected wave off of the bottom of the ground plane, thereby allowing an electric-type antenna to be used in close proximity to the ground plane that shields it, and allowing for a lower-profile surface mounted antenna.

For the ol' folks at home

ACKNOWLEDGEMENTS

I would like to thank Dr. Leo Kempel for his guidance through my career at Michigan State. I thank him for giving me the opportunity to attend Michigan State, and for his mentoring during my career here. I would like to thank Dr. Ed Rothwell for his wise tutoring and patience. I would like to thank Dr. Dennis Nyquist for his bottomless pool of electromagnetic knowledge.

A thanks to Dr. Stephen Schneider and Capt. Keven Golla of the Air Force Institute of Technology for their support for and work on this project.

I thank Dr. John Burke, formerly of Mission Research Corp. and now an assistant professor at Western New England College. John, it was your guidance and mentoring at MRC that sparked an interest in me for electromagnetics, and ultimately led me to pursue a higher degree.

A special thanks to my wonderful family for their support, patience and positive attitudes while I worked to attain this degree. I have been blessed in so many ways, and I am so happy to have the opportunity now to spend more time with all of you. Finally, to my girlfriend Kristen and her family: thank you for your support and all you have done for me in the past few months. The gloomy days in Mid-Michigan have been brighter because of you.

TABLE OF CONTENTS

LIST OF TABLES	vii
LIST OF FIGURES.....	viii
CHAPTER 1	1
INTRODUCTION.....	1
1.1 Problem Statement	1
1.2 Overview	3
CHAPTER 2	5
HISTORY OF HIGH IMPEDANCE GROUND PLANES	5
2.1 Problems With Conventional Conformal Antennas	5
2.2 Photonic Band Gaps.....	9
2.3 High-Impedance Ground Planes.....	15
2.4 Electric Source Antennas (Type 1) and High Impedance Ground Planes	21
2.5 Magnetic Source (Type 2) Antennas and High Impedance Ground Planes..	28
2.6 Summary.....	34
CHAPTER 3	36
COMPUTATIONAL RESULTS OF PREVIOUSLY BUILT STRUCTURES	36
3.1 Method of analysis	36
3.2 Wideband Hexagonal Patch with Normal Dielectric Border	40
3.3 Wideband Patch with HIGP Border.....	46
3.4 Wideband Patch with PEC border	51
3.5 Conclusions	53
CHAPTER 4	54
PROPOSED FOUR LAYER ANTENNA/HIGP DESIGN METHOD	54
4.1 Introduction	54
4.2 Bowtie Dipole over HIGP Substrate.....	56
4.3 Bowtie Dipole over Grounded Dielectric Substrate	68
4.4 Optimized Bowtie Dipole/HIGP Design.....	72
4.5 Proposed Design not Computationally Tested	81
CHAPTER 5	84
CONCLUSIONS AND GROUNDS FOR FUTURE WORK.....	84
APPENDIX A	88
CREATING INPUT FILES FOR PRISM.....	88
A.1 Methodology	88
A.2 ReadXYZ Fortran Code for Reading DXF2XYZ Ouptut.....	97

REFERENCES..... 101

LIST OF TABLES

Table A-1: Sample Output from DXF2XYZ.....	90
Table A-2: Sample Skymesh .pts File	92
Table A-3: Sample Skymesh .edg File	93
Table A-4: Sample Skymesh .ref File	94
Table A-5: Sample Skymesh .prj File	94
Table A-6: Flowchart for Creating the Prism Input Files.....	96

LIST OF FIGURES

Figure 2-1: Printed probe-fed bowtie dipole on dielectric substrate.....	6
Figure 2-2: Cavity-Backed Printed Type I Antenna Configuration.....	7
Figure 2-3: E-plane pattern of a printed dipole over dielectric slab	8
Figure 2-4: Actual and Imaged Sources Above Perfect Electric (PEC) and Perfect Magnetic (PMC) Conductors	9
Figure 2-5: Patch antenna (left) and printed dipole (right) over PBG substrates	10
Figure 2-6: Radiation pattern of a bowtie-dipole over PBG substrate.....	11
Figure 2-7: Microstrip-fed Patch.....	12
Figure 2-8: Surface Fields for Microstrip-fed Patch	12
Figure 2-9: Microstrip-fed Patch with PBG Border.....	13
Figure 2-10: Surface fields for Microstrip-fed Patch with PBG Border	13
Figure 2-11: Hexagonal-based HIGP surface	16
Figure 2-12: HIGP Geometry	17
Figure 2-13: Reflection Phase of a Wave from a Resonant HIGP.....	18
Figure 2-14: TM Surface Wave Measurements of a Flat Copper Sheet (a) and a HIGP Surface (b).....	20
Figure 2-15: Wideband Zigzag Dipole Over a Wideband HIGP structure	22
Figure 2-16: Probe-fed Monopole Over HIGP surface	22
Figure 2-17: Broadside Transmission Measurement of a Wideband Zigzag Antenna over Wideband HIGP surface	25

Figure 2-18: Broadside Frequency Response of Copper Tape Monopoles Connecting 4 HIGP Elements, with and without Vias.....	27
Figure 2-19: Wideband Hexagonal-Based Patch Antenna	28
Figure 2-20: Wideband Patch with HIGP Border	29
Figure 2-21: Wideband Patch with PEC border	31
Figure 2-22: Broadside Transmission Measurement of Hexagonal Based Wideband antennas with three different borders	33
Figure 3-1: A sample finite element model of a square patch.....	38
Figure 3-2: Sample Mesh for Wideband Patch used from 2-4 GHz.....	41
Figure 3-3: Input Impedance of Wideband Hexagonal-based Patch with simple Dielectric Border.....	42
Figure 3-4: Normalized tangential (a) and z-directed (b) substrate-level E-field strength for hex-based wideband patch antenna at 4.4186 GHz.....	43
Figure 3-5: Normalized tangential (a) and z-directed (b) substrate-level E-field strength for hex-based wideband patch antenna at 6.2685 GHz.....	44
Figure 3-6: Mesh used for Wideband Patch with HIGP border from 2-4 GHz.....	47
Figure 3-7: Input Impedance for Wideband Patch with HIGP border	48
Figure 3-8: Normalized Tangential (a) and Z-directed (b) Substrate-Level E-field Strength for Wideband Patch with HIGP Border at 4.32645 GHz.....	50
Figure 3-9: Input Impedance for the Wideband Patch with PEC Border.....	52
Figure 4-1: A Bowtie Antenna with HIGP Substrate.....	56
Figure 4-2: Cross Section of Proposed Four-Layer Design for a Dipole over a HIGP Substrate.....	57

Figure 4-3: Measured Resistance (a) and Reactance (b) vs. Electrical Length for Triangular Dipole with 60° Flare Angle (from [13])	61
Figure 4-4: Computed Input Impedance for the Bowtie Antenna with HIGP substrate ...	63
Figure 4-5: Expanded view of Input Impedance of Bowtie Dipole over HIGP substrate from 4.2 – 5GHz.....	64
Figure 4-6: Bowtie Dipole with HIGP-Substrate with Reduced Number of Elements	66
Figure 4-7: Input Impedance of Bowtie Dipole with Reduced-Size HIGP Substrate.....	67
Figure 4-8: Diagram of a Printed Bowtie over Grounded Dielectric Substrate.....	68
Figure 4-9: Input Impedance of a Probe-fed Bowtie Antenna over Grounded Dielectric Substrate.....	70
Figure 4-10: Expanded Input Resistance of the Bowtie over HIGP and Grounded Dielectric Substrate from 4.2 – 5.0 GHz	71
Figure 4-11: Input Resistance for Bowtie Antenna over HIGP and Grounded Dielectric Substrates	74
Figure 4-12: Broadside Normalized E-plane Pattern (gain, db) of the Bowtie Antenna with HIGP Substrate and Grounded Dielectric Substrate, F=5.58 GHz	77
Figure 4-13: Broadside Normalized H-plane Pattern (gain, db) of the Bowtie Antenna with HIGP Substrate and Grounded Dielectric Substrate, F=5.58 GHz	78
Figure 4-14: Normalized Tangential (a) and z-Directed E-fields for Antenna over HIGP Substrate.....	79
Figure 4-15: Normalized Tangential (a) and z-Directed E-fields for Antenna over Grounded Dielectric Substrate	80
Figure 4-16: Untested Antenna/HIGP Four Layer Design.....	81

Figure A-1: Square Patch Drawn in CAD	89
--	-----------

CHAPTER 1

INTRODUCTION

1.1 Problem Statement

Antennas can generally be classified into two categories: electric current (Type 1) and equivalent magnetic current or aperture (Type 2) antennas [1]. In surface mount applications, as in the skin of an aircraft, both these types of antennas require a reflector or ground plane of some sort. A printed dipole (Type 1), for example, requires a ground plane or reflector to direct radiation into a particular half-space, usually in the form of an absorber-loaded quarter-wave cavity. A patch antenna (Type 2) requires a ground plane to direct the electromagnetic wave to its radiation point. The finite ground plane in both these cases is known to have negative effects on the performance of the antenna. In the past thirteen years, there have been developments in optics, physics and electromagnetics that have proven to alleviate some of the issues with antenna ground planes. These developments include the discovery of photonic band gaps (PBG) [2] and high-impedance ground planes (HIGP) [3].

A photonic band gap is a band of frequencies for which electromagnetic waves do not propagate in a particular medium. A HIGP is a device that utilizes PBG theory to create a structure that forbids the flow of surface waves. HIGPs also have the interesting property that they reflect incident electromagnetic energy with no phase reversal when the incoming wave is within the PBG of the surface. There have been numerous efforts to improve the bandwidth of the HIGP, i.e., increase its PBG [4].

The purpose of this thesis is, first, to shed light onto the operation of a HIGP in the RF/microwave range. Computational results have been obtained on a number of hybrid HIGP/planar antenna structures using a custom Finite Element Method (FEM) code called Prism [5]. With this code, the fields inside the aperture and under the HIGP surface can be analyzed. The normal and tangential (with respect to the surface of a planar antenna) electric fields for several antennas are plotted. These plots provide valuable insight to how a HIGP/planar antenna structure works at resonance. Secondly, it is shown how a high-impedance ground plane can help to reduce the overall volume that a surface-mounted antenna consumes, and can even improve the performance of the antenna. A novel four-layer design concept for a hybrid HIGP/antenna structure is introduced. This design has the advantage of being low-profile in volume and surface area, and fairly well matched over a broad band ($\sim 28\%$). This concept places a wideband electric/real source antenna in the form of a bowtie-dipole parallel and in close proximity to a HIGP surface. It is seen how this concept enhances the performance of dipoles placed near the ground plane that shields them, thus making the printed dipole more conducive to surface-mounting environments.

1.2 Overview

The next chapter will highlight the history and operation of PBG structures and HIGP's. In chapter two, the applications of HIGP's to planar antennas will be presented, and their advantages to the operation of these antennas will be discussed. Chapter two will also explain work that has been done to make the HIGP more broadband. Chapter three will present results from computational analysis of some hybrid antenna/HIGP structures that have previously been built and tested at the Air Force Institute of Technology. In chapter four, a new design concept is presented in order to improve the bandwidth of a HIGP/antenna combination. This concept uses electric-type antennas separated from a HIGP surface by a thin layer of dielectric material. It is the goal of this thesis to present and analyze this new design concept for planar antenna/HIGP structures. Because the design equations for these structures treat the surface as a lumped surface impedance made of periodic elements, implicit in the design is that the periodicity of the surface is much smaller than the wavelength of operation, i.e., that many more than one HIGP element exist per wavelength. This places a large burden on computational design and the subsequent analysis, which requires that the mesh which represents the structures consist of triangular elements that are at least $\lambda/15 - \lambda/20$ in spacing, or smaller. Therefore, a high number of HIGP elements translate into a high number of surface triangles that are used to represent those elements, leading to huge memory requirements and even more extreme computation and solution time. Some of the meshes used for this work took up to five weeks for a medium-resolution frequency sweep. Therefore, a secondary goal of this work is to determine how few HIGP elements can be used to create

the surface and yet still behave well as a high-impedance ground plane. This knowledge, coupled with the design concept presented in chapter four, can lead to streamlined HIGP structures that are low-profile in both volume and surface area, are easy to build due to the low number of elements, and yet still yield surface-mounted electric-type antennas that are well matched to a $50\ \Omega$ transmission line. Therefore, though the new structures and design concepts presented here are certainly not optimized and complete, they open the door to a new way of designing and building HIGP/planar antenna combinations.

In chapter five, some grounds for future work are presented. This involves several concepts to aid or even enhance the design process and the computational analysis used to predict the performance of HIGP surfaces.

CHAPTER 2

HISTORY OF HIGH IMPEDANCE GROUND PLANES

2.1 Problems With Conventional Conformal Antennas

The patch antenna is a versatile, lightweight antenna used in many applications, from handheld GPS receivers to electronic warfare (EW) systems and radars on aircraft surfaces. The patch can radiate energy in almost any direction in a half-space. This antenna requires a ground plane to concentrate energy under the patch and out to the edges where it is radiated (e.g., the cavity model). The normal AC image currents on the ground plane created from the radiating element can have negative effects on the antenna itself or on other surrounding devices. If the ground plane or cavity is placed too close to the antenna, surface waves traveling on the dielectric substrate will partially reflect from the ground plane and travel back to the antenna, thus drastically changing the input impedance of the antenna. If the perimeter of the ground plane is truncated too quickly, the normal AC image currents coupled to the ground plane from the antenna will have enough energy to radiate into space when they encounter a discontinuity, such as the edge of the ground plane. This radiation can alter the pattern and gain significantly. If enough power is input to the antenna, surface currents can couple to surrounding objects, such as wingtips or discontinuities in an aircraft skin, and radiate. The common solution to this problem is to make the ground plane bigger, so that surface currents will attenuate in the imperfect metal before they reach an edge. This generally requires a ground plane that extends several wavelengths out from the antenna at the lowest operating frequency,

which can substantially increase the amount of real estate required for the antenna to operate efficiently.

A known problem with the patch is that it is very narrowband and has relatively low gain, even at resonance. Electric type antennas, such as bowtie dipoles, spirals, or log-periodics can have tremendous broadband behavior with equally impressive gain and suitable patterns. However, these real-source antennas do not lend themselves well to surface-mount environments. These antennas rely on an electric field that is parallel-polarized to the plane in which the antenna lies. They radiate out in both directions parallel to the antenna, as in Figure 2-1.

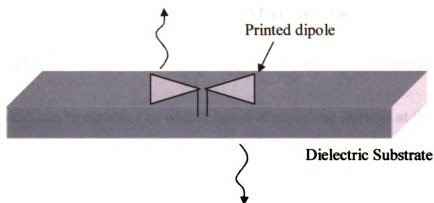


Figure 2-1: Printed probe-fed bowtie dipole on dielectric substrate

In a surface-mount environment, the radiation extending through the substrate and to the back side can interfere with other devices, such as electronics or radars, or can couple to other radiating elements and increase the radar cross section of the vehicle tremendously. The solution to this problem is to place a shield behind the antenna to protect these devices, typically in the form of a quarter-wave cavity at the center frequency. This configuration is shown in Figure 2-2. The cavity-backed antenna, however, can be extremely narrowband, significantly reducing the bandwidth of a normally broadband

antenna, as in the bowtie. The fields reflected by the bottom of the cavity interact with the field at the feed and make the antenna appear as a short circuit at frequencies other than where the cavity depth is a quarter-wavelength.

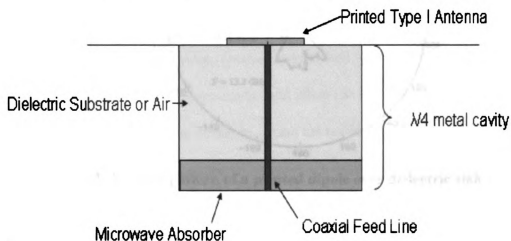


Figure 2-2: Cavity-Backed Printed Type I Antenna Configuration

The bandwidth can be extended by adding layers of absorbing material at the bottom of the cavity, attenuating the field transmitted down to the cavity bottom, and again after the wave has been reflected. However, the absorber reduces the total available power for radiation. The most obvious problem with the quarter wave cavity is that it requires significant real-estate in the backward half-space, precluding its use in surface mount environments. Finally, the fields tend to concentrate in the dielectric region of a printed electric-type antenna, instead of radiating into free space. For a higher dielectric material, the fields become more coupled to surface waves in the dielectric substrate than to plane waves in free space. Figure 2-3 shows the E-plane pattern of a printed dipole antenna over a non-grounded dielectric substrate. It is clear that most of the radiation extends out through the substrate and then into space, instead of into space directly.

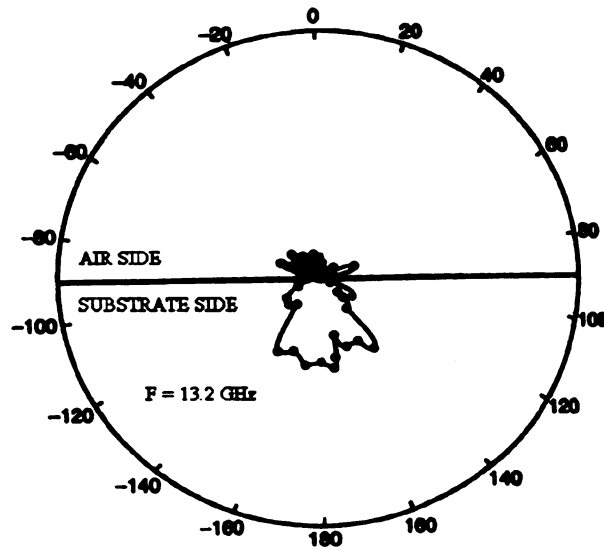


Figure 2-3: E-plane pattern of a printed dipole over dielectric slab (from [7])

The problems presented here in the design of planar antennas can be alleviated by the use of photonic band gap (PBG) technology and high-impedance ground planes (HIGP). The discovery of photonic band gaps in 1989 has allowed for many developments in microwave and antenna engineering. The high-impedance ground plane is an extension of the study of PBG's, in that the HIGP is treated as a lumped surface impedance in a macroscopic sense. The history of these two fields will be presented next.

2.2 Photonic Band Gaps

A photonic band gap (PBG) structure, also called a high-impedance ground plane (HIGP) when used in the RF-microwave range, is a device that suppresses tangentially traveling electromagnetic energy (surface waves) and reflects incident energy with no phase reversal in the tangential electric field when the frequency of the energy is within the photonic band gap of the structure. When the reflected electric field has no phase reversal, the surface acts as a magnetic conductor, complementary to the phase reversal of the electric field in an electric conductor.

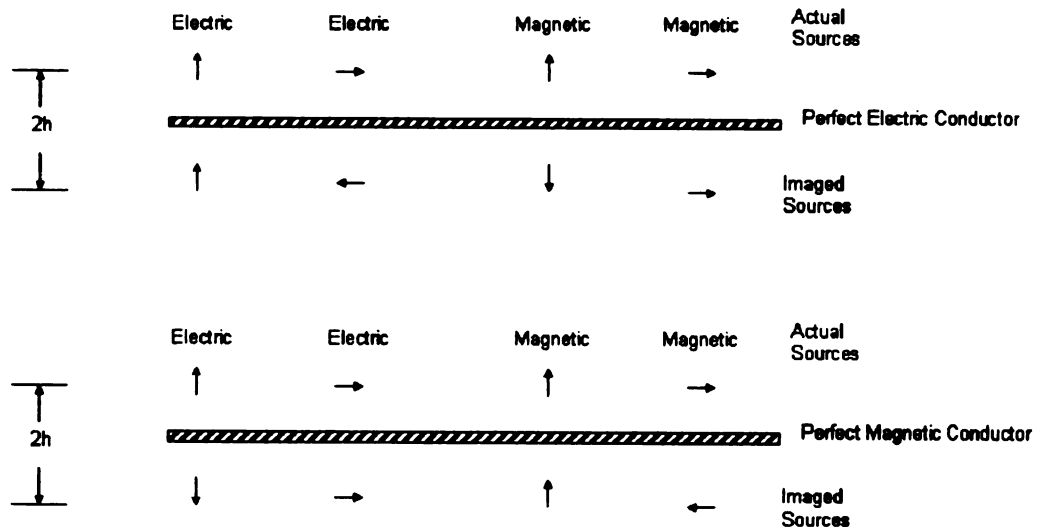


Figure 2-4: Actual and Imaged Sources Above Perfect Electric (PEC) and Perfect Magnetic (PMC) Conductors (from [6])

The real electric current flowing along the surface of an electric conductor is replaced by a fictitious magnetic current when the analogy is extended to magnetic conductors. This is summarized in Figure 2-4.

In the early analysis of PBG's, much attention was devoted to formulating analogies between the PBG structure and a crystal or molecule, and to understanding the interactions between an electromagnetic wave and the entities comprising the crystal. By using band theory of photons, a structure can be designed which forbids the flow of light through the structure. The first PBG structure, developed by Yablonovitch, was a small cube of dielectric material with spherical pockets of air embedded in it in a grid fashion. Yablonovitch found that this structure forbids the flow of electromagnetic waves over a significant bandwidth (14%) [2].

Since this original study, many researchers have incorporated PBG structures into the design of planar antennas [7,8,9,10,11]. Figure 2-5 shows a patch antenna surrounded by, and a printed dipole on top of, a PBG substrate.

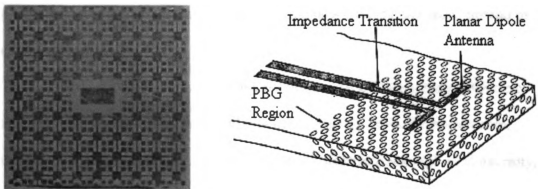


Figure 2-5: Patch antenna (left, from [10]) and printed dipole (right, from [7]) over PBG substrates

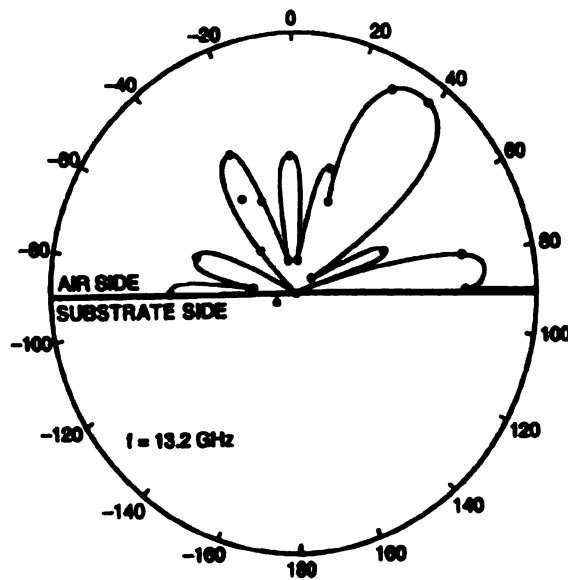


Figure 2-6: Radiation pattern of a bowtie-dipole over PBG substrate (from [7])

Gonzalo and others found that the patch surrounded by PBG substrate was effective at suppressing surface waves and improving the gain compared to a normal patch with dielectric border [11]. Brown found that the dipole, when operated over the PBG substrate, exhibited far better performance than when operated over the high-dielectric substrate. Figure 2-6 shows the radiation pattern of the dipole over a PBG substrate. Comparing to Figure 2-3, it is clear that the radiation now extends into space instead of through the dielectric.

Figure 2-7 shows a typical microstrip-fed patch surrounded by grounded dielectric substrate. Figure 2-8 shows a surface field plot of the electric fields for this structure when operated at a frequency of 2.14 GHz. The bright areas indicate high field intensity, while the dark areas indicate low field intensity. Notice the areas of high field intensity around the transmission line and the center of the patch, but also at points away from the patch. Figure 2-9 is the same patch but with a PBG structure border.

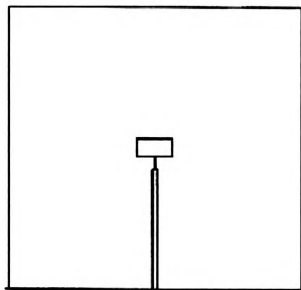


Figure 2-7: Microstrip-fed Patch

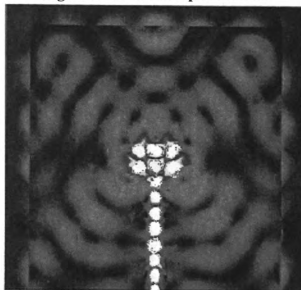


Figure 2-8: Surface Fields for Microstrip-fed Patch

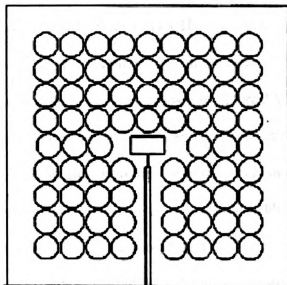


Figure 2-9: Microstrip-fed Patch with PBG Border

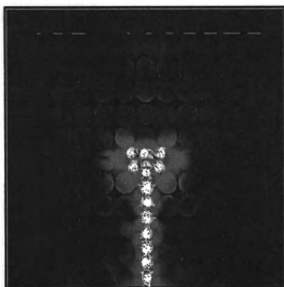


Figure 2-10: Surface fields for Microstrip-fed Patch with PBG Border

*Figures Figure 2-7, Figure 2-8, Figure 2-9, and Figure 2-10 are from [11]

The PBG structure consists of air columns embedded in a dielectric material ($\epsilon_r = 10$) in a lattice-like fashion. Figure 2-10 shows the surface fields for this structure when operated at the same frequency as the normal patch, 2.14 GHz. The intensity of the surface fields has clearly been reduced at points other than in the immediate vicinity of the patch. Looking forward to later chapters, the design shown in Figure 2-9 is one on which the novel designs in this thesis are based, in that the air columns that comprise the surface are spaced roughly a distance apart similar to the size of the patch, indicating that the periodicity is on the order of the wavelength of the radiated fields.

Sievenpiper found that a PBG structure could be described in a macroscopic sense, using surface impedance models to predict the behavior of the structure. This progression of research has formed a new topic and new method of analysis in PBG structures: the high impedance ground plane.

The co

found

be ana

much

LC cir

imagin

acts as

the inc

propag

Sie

the sh

of the

2.3 High-Impedance Ground Planes

The concept of a high-impedance ground plane was first presented by Sievenpiper [3]. He found that photonic band-gap structures consisting of periodic elements of some sort can be analyzed using a surface impedance model as long as the periodicity of the structure is much smaller than a wavelength. This analysis treats the entire PBG surface as a resonant LC circuit, with an appropriate center frequency and bandwidth. At some frequency, the imaginary part of the surface impedance goes to infinity. At this frequency, the surface acts as a magnetic conductor, in that the reflected tangential electric field is in phase with the incident field. In some band around this center frequency, neither TM nor TE modes propagate along the surface as waves.

Sievenpiper found that in a high impedance surface comprised of periodic elements, the sheet capacitance and inductance can be described in terms of the physical parameters of the sheet. Figure 2-11 is an example of a periodic hexagonal based HIGP surface.

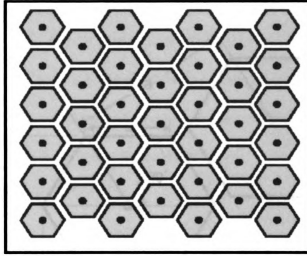


Figure 2-11: Hexagonal-based HIGP surface

The capacitance of the surface comes from the charge separation on adjacent metal pads across the dielectric substrate. The black circles in the middle of each pad represent metal vias connecting the pads to a continuous copper conducting ground plane on the back side of the surface, with some dielectric substrate in between. The sheet inductance comes from currents traveling from the pads on the top layer down through these vias, across the bottom ground plane and looping around to the via of an adjacent pad. The capacitance of an individual element is found from conformal mapping to be

$$C_{element} = \frac{w\epsilon_0(\epsilon_{r,1} + \epsilon_{r,2})}{\pi} \text{Cosh}^{-1}\left(\frac{a}{g}\right) (\text{Farads / square}) \quad (2.1)$$

where w is the edge length of an element, $\epsilon_{r,i}$ is the relative permittivity of the ambient media (usually free space, but can be dielectric for multi-layer applications as will be seen later), $\epsilon_{r,2}$ is the permittivity of the dielectric substrate immediately beneath the metal pads, a is the center to center spacing of elements and g is the gap that exists

between adjacent elements. The geometry of the structures Sievenpiper used is shown below in Figure 2-12.

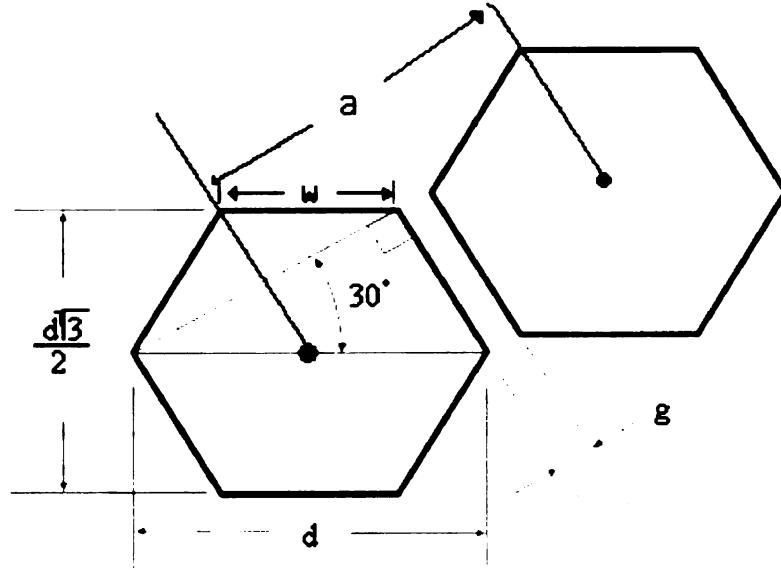


Figure 2-12: HIGP Geometry

The capacitance of an individual element is multiplied by a geometrical correction factor to obtain the sheet capacitance, which accounts for the grid-like nature of the elements. In the case of hexagonal elements, the geometrical correction factor is $1/\sqrt{3}$. The sheet inductance, in Henrys/square, is found by integrating the magnetic field around a solenoidal loop. It is given by

$$L_{sheet} = \mu_o \mu_r t (\text{Henrys / square}) \quad (2.2)$$

where μ_o is the permeability of free space, μ_r is taken to be 1.0 for non-magnetic substrates, and t is the thickness of the dielectric.

The result of a measurement of the phase of the reflected fields from the HIGP surface is shown in Figure 2-13. The phase of the reflected wave from the HIGP surface, referenced to the phase of the incoming wave, travels from π radians, through 0 and to $-\pi$

radians. This measurement consisted of performing a mono-static reflection measurement of a large metal sheet in an anechoic chamber for calibration purposes, and then of a HIGP. The HIGP data was divided by that of the metal sheet to calibrate, and a phase shift of π was added back in to account for the phase of the metal sheet. An infinite perfect metal conductor would have a phase shift of π or $-\pi$ radians when referenced to the phase of the incoming wave across the entire RF band.

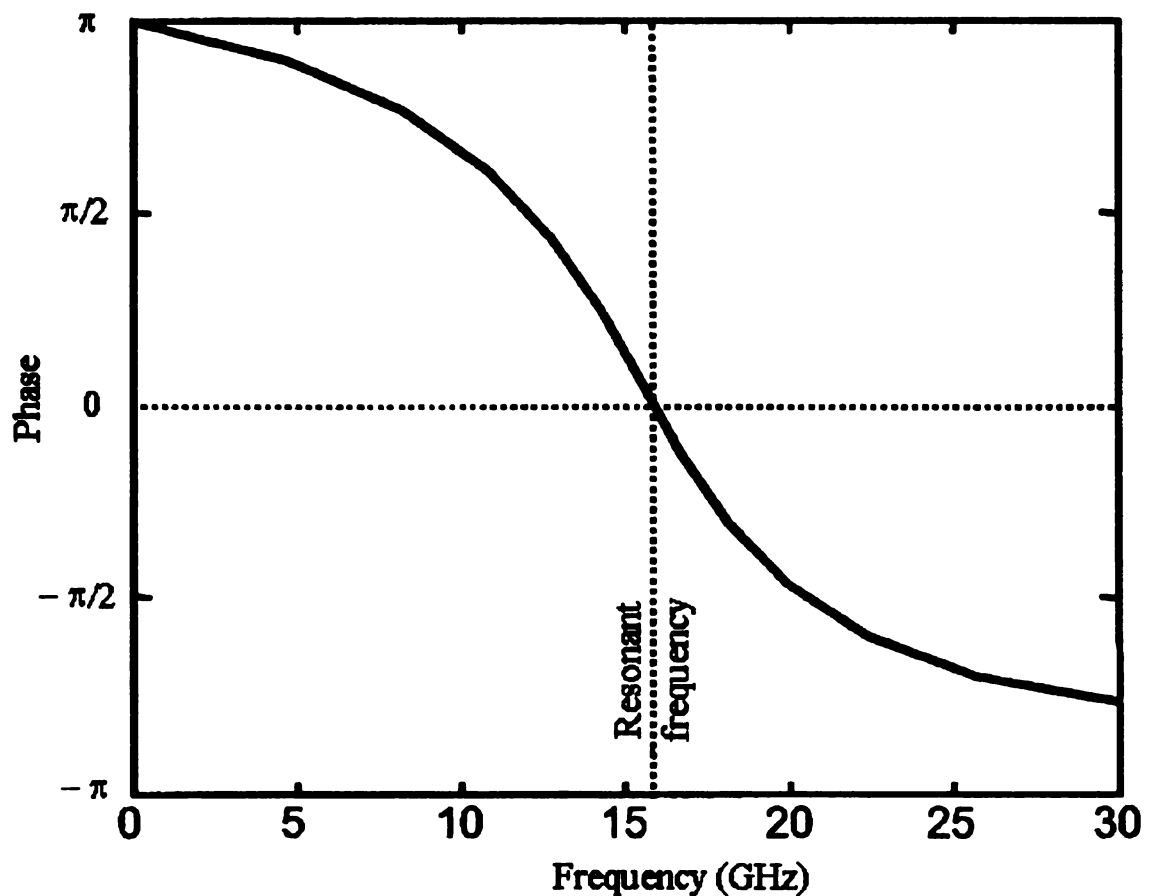
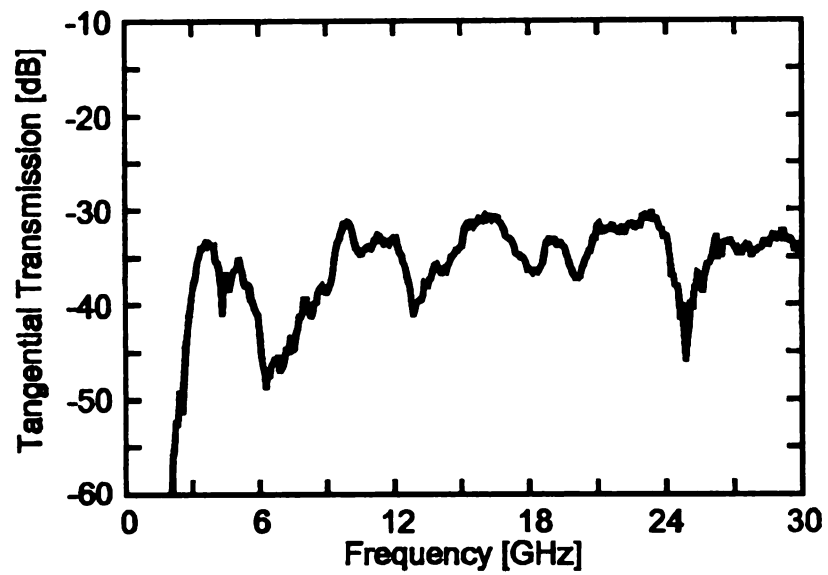
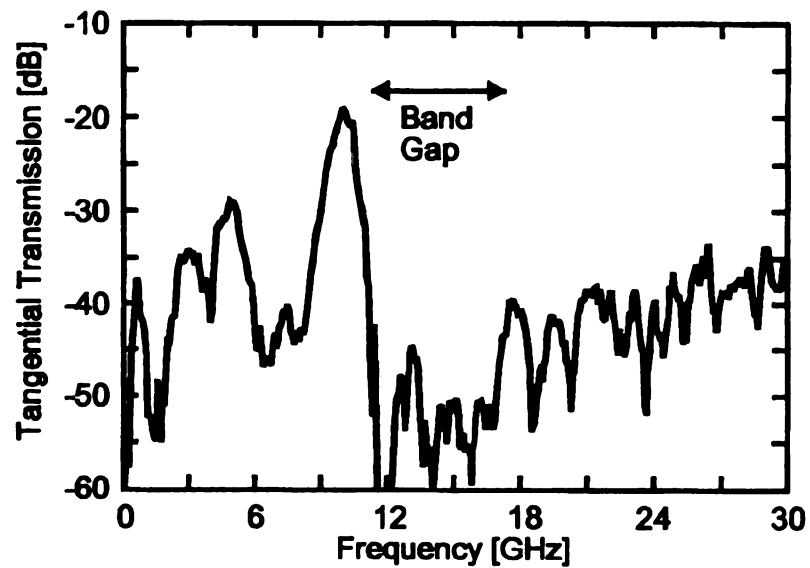


Figure 2-13: Reflection Phase of a Wave from a Resonant HIGP (from [3])

The surface wave measurements were performed by inducing TM and TE surface waves on both a flat metal sheet and then across a HIGP surface. The measurement had to be performed at frequencies at which surface waves could be coupled to the lossy metal sheet, starting at roughly 2 GHz. Two small monopole probes (T_x and R_x) were placed vertically on both sides of the flat metal sheet or the hexagonal-based HIGP. The vertical electric field launched by the probe couples to the vertical electric field of a TM surface wave. The experiment was repeated with the probes oriented parallel to the surfaces in order to couple to the parallel electric field of a TE surface wave. The results of the TM measurements are shown in Figure 2-14. The PBG for this high-impedance surface exists between 12 and roughly 17 GHz.



(a)



(b)

Figure 2-14: TM Surface Wave Measurements of a Flat Copper Sheet (a) and a HIGP Surface (b) (from [3])

2.4 Electric Source Antennas (Type 1) and High Impedance Ground Planes

High impedance ground planes can be used in conjunction with planar antennas to produce some useful antenna characteristics. It was found that monopole antennas could be placed parallel at a very small distance ($< \lambda/4$) from a HIGP and still operate well. This means that electric type antennas can be placed very near a reflecting ground plane, allowing for efficient radiation into one half-space without consuming too much volume. Golla tested several electric type antennas, in the form of zigzag dipoles and copper-tape monopoles placed directly above a HIGP structure [4]. These structures are shown in Figure 2-15 and Figure 2-16.

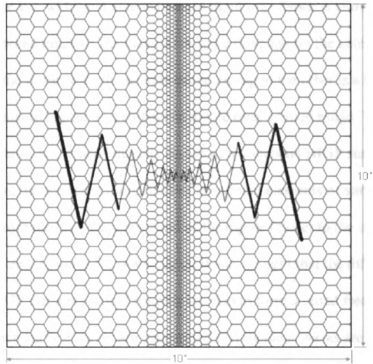


Figure 2-15: Wideband Zigzag Dipole Over a Wideband HIGP structure

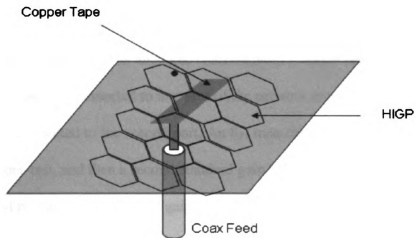


Figure 2-16: Probe-fed Monopole Over HIGP surface

*Figure 2-15 and Figure 2-16 are from [4]

The zi

consta

at poin

making

made

seen i

elemen

lower

range

opera

phase

dipo

anter

mea

mea

stan

und

ante

ther

per

The

rac

tra

The zigzag dipole is a wideband antenna whose input impedance is known to stay fairly constant over a broad range of frequencies. A wave traveling on the antenna will launch at points where the distance from one side of the zigzag to the other is a half-wavelength, making the antenna to appear as a half-wave dipole over a broad range. This antenna, made of copper tape, was placed directly on top of a wideband HIGP surface. As can be seen in the figure, the surface is comprised of hexagonal elements of varying sizes. These elements scale from the high-frequency end of the dipole (closer to the center) to the lower frequency end, towards the outer edges. It was thought that the different frequency ranges of the HIGP elements would roughly overlap to form a broad frequency band of operation in which surface waves are suppressed and incident waves are reflected with no phase reversal. This band of frequencies should fall within the operating range of the dipole to form a well tuned antenna/HIGP structure. However, Golla found that this antenna did not perform well. Figure 2-17 is the broadside frequency response (S_{21}) measurement of this antenna. These measurements are standard S_{21} transmission measurements performed in an anechoic chamber with a vector network analyzer. A standard gain horn is connected to one port of the network analyzer and the antenna under test is connected to the second port. An S_{21} measurement is performed on both the antenna-under-test, and then a second standard gain horn. The antenna-under-test data is then divided by that of the standard gain horn data in order to calibrate. The antenna performs worse than an isotropic radiator over nearly the whole measurement range. There is a band around 15 GHz however that does perform better than an isotropic radiator. Golla attributes the poor performance to the HIGP surface suppressing the traveling wave on the dipole in all bands but the high-frequency band that is radiated

from the small region close to the feed. The desirable surface wave suppression that is usually associated with HIGP appears to hinder the performance of a broad band, traveling wave antenna. However, the experiment was performed by placing the zigzag antenna directly over the HIGP surface, with only a negligible film of adhesive that is found on the back of copper tape separating the antenna from the HIGP surface. It is quite possible that the extremely small separation distance between the antenna and the HIGP surface causes the antenna to short directly to the HIGP elements themselves. In Chapter 4, an antenna is presented that uses the same design principle, a broadband electric-type antenna over a HIGP surface. However, the separation between the antenna and the HIGP surface is more significant, .059 mils (1 mil = .001") or 1.5 mm. This design has the desired qualities of a broadband antenna yet requires less volume and surface area than the current design methodology would require for this type of antenna.

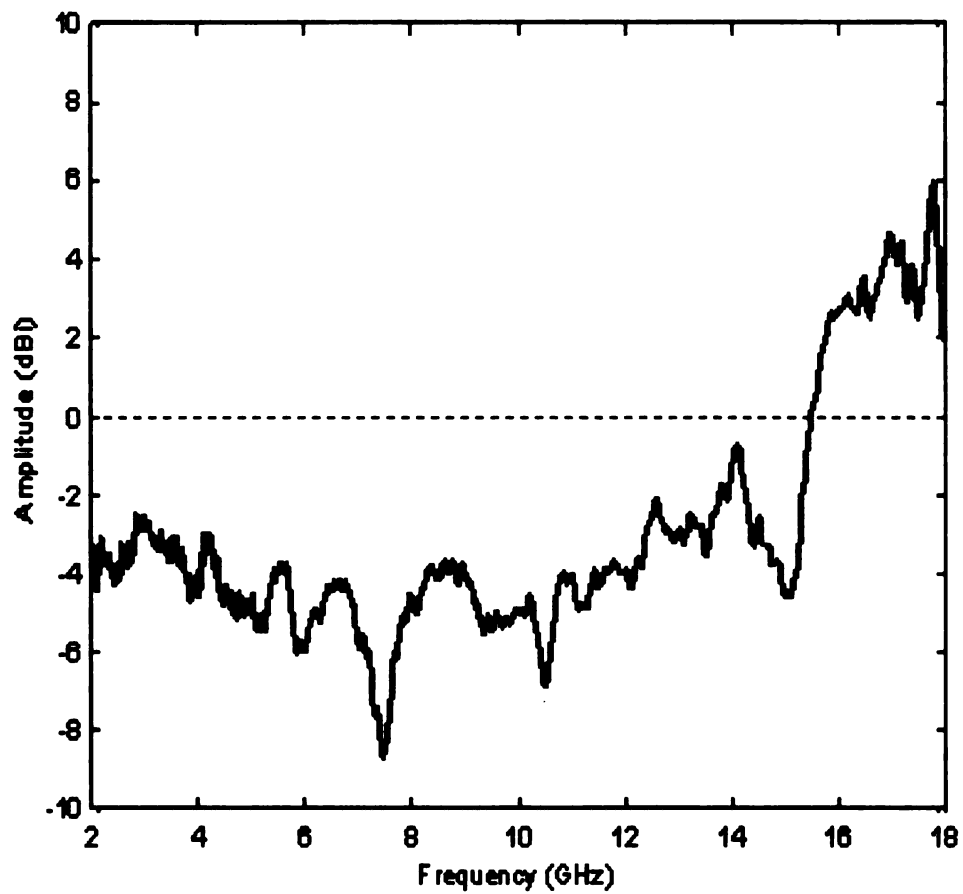


Figure 2-17: Broadside Transmission Measurement of a Wideband Zigzag Antenna over Wideband HIGP surface (from [4])

The copper tape monopole was also placed directly adjacent to the HIGP surface. In this experiment, the goal was to actually create an antenna from the HIGP elements themselves. The copper tape stretches from the coaxial probe feed across the HIGP surface and connects one or more HIGP hexagonal pads together. Because the conducting vias in a typical HIGP surface provide a shorting path to ground, they were removed for this experiment. It was found that a monopole connecting together 4 of the HIGP pads performed reasonably well over a small band. The experiment was then repeated with the conducting vias in place, except for the vias in the elements directly below the antenna (leaving these vias intact would have shorted the antenna directly to the ground plane underneath). Figure 2-18 is the broadside frequency response (S_{21}) of the copper tape monopole linking together 4 of the elements. Both antenna structures have bands in which they perform better than an isotropic radiator. These bands are fairly narrow, and the maximum received signal even at best is only 2 dbi. This experiment did prove, however, that the HIGP elements could be used as antennas. This led to the development of integrated antennas that married together the HIGP elements and the antenna itself, so that one or more HIGP elements were probe-fed as patches in the same plane as the HIGP surface, creating an extremely low profile surface mounted antenna.

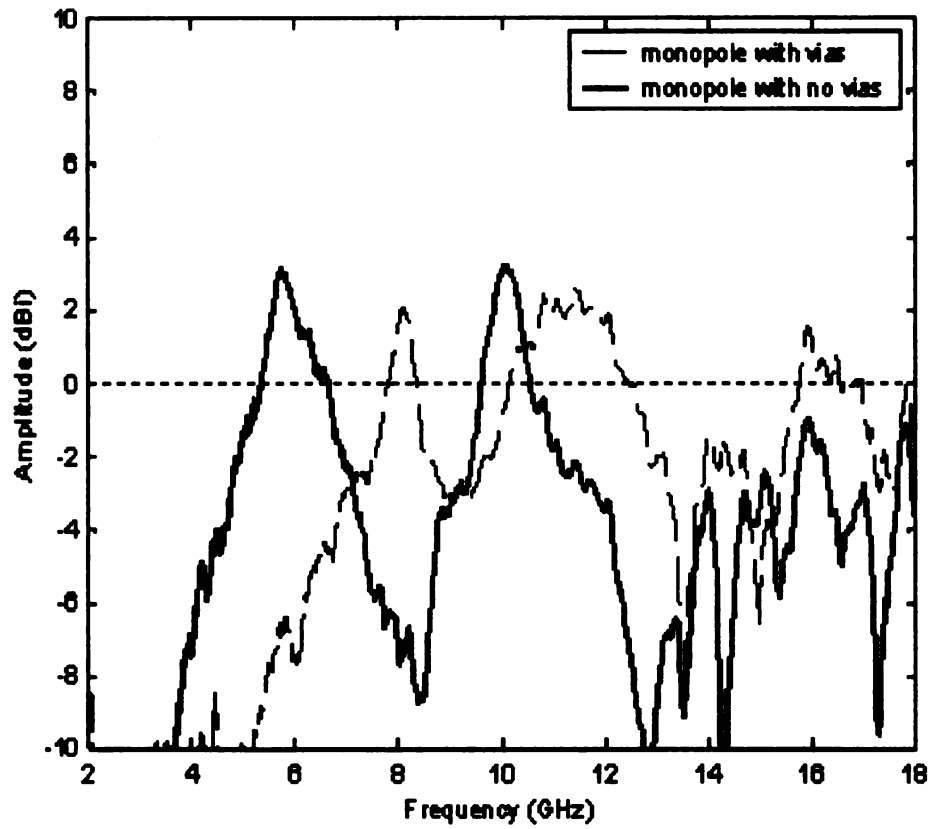


Figure 2-18: Broadside Frequency Response of Copper Tape Monopoles Connecting 4 HIGP Elements, with and without Vias (from [4])

2.5 Magnetic Source (Type 2) Antennas and High Impedance Ground Planes

It was found that patch antennas could be placed in the plane of the HIGP surface and radiate well, without the surface waves that are normally a byproduct of a patch antenna. This was seen in Figure 2-5 where the patch is adjacent to the HIGP elements. Golla did work in trying to increase the bandwidth of a HIGP/patch antenna hybrid design. He fabricated the antenna itself out of the same elements that make up the HIGP, using a superposition of different sizes of hexagonal pads. The antenna by itself is shown below, in Figure 2-19.

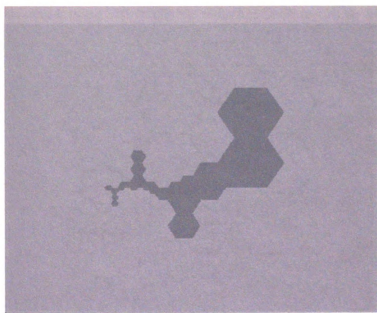


Figure 2-19: Wideband Hexagonal-Based Patch Antenna

The antenna consists of hexagonal pads of different sizes, with the design philosophy that the different sizes will radiate at different frequencies. There are four different sizes of

metal pads shown here, with the dimensions of each unique pad size increasing linearly by a factor of two. The base hexagonal unit is 120 mils in diameter. From equation 2.1, the element-to-elements spacing (a) is 114 mils, the gap width (g) is 10 mils, the edge-length (w) of an element is 60 mils, and the substrate on which the structure is printed is FR4 of thickness 59 mils with a dielectric constant of 4.9. The aperture size (large square of dielectric surrounding the patch) is 2.5" x 2.5". The goal of his work was to then build an appropriately sized HIGP that would fit around this antenna and suppress surface waves, reduce the aperture size and yet still allow the antenna to radiate well over a large band of frequencies. The antenna with the HIGP border is shown below in Figure 2-20.

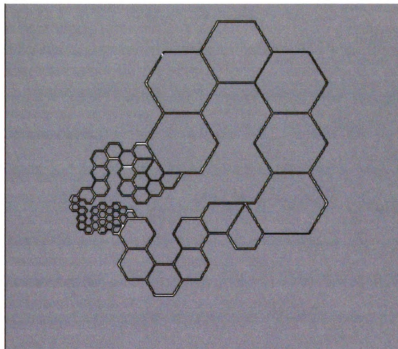


Figure 2-20: Wideband Patch with HIGP Border

The HIGP elements wrap around the antenna, so that the entire aperture size now shows a significant reduction compared to that of the dielectric border. The dark lines surrounding the metal pads and the antenna represent dielectric substrate. The HIGP surface for this antenna scales in size linearly with the sizes of the metal antenna elements create theoretical wideband HIGP surface. The third antenna tested in this series was an extreme-case scenario: the dielectric border of Figure 2-19 border was shrunk so that there was only a small 10 mil gap separating the antenna from the surrounding PEC surface, shown in Figure 2-21. This structure has the smallest aperture size possible, in that the metal surrounding the antenna, which could, in a surface mount environment, represent the fuselage of an aircraft or the nosecone of a missile, is now nearly directly adjacent to the antenna leaving little room for radiation fields to escape from beneath the patch.

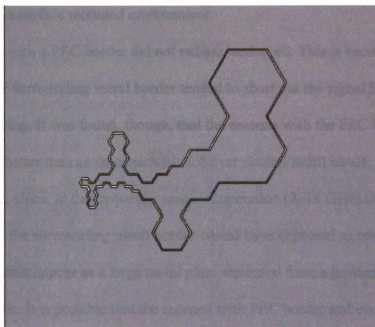


Figure 2-21: Wideband Patch with PEC border

Golla performed broadside transmission measurements of these three antennas. The results of these measurements are shown in Figure 2-22. He found that the antennas with the dielectric border and the HIGP border radiated better than an isotropic radiator over a very significant bandwidth. In fact, the antenna with the HIGP border outperformed the antenna with dielectric border at certain frequencies. This indicates that a patch antenna with a small aperture can still perform well over certain bands. The significance of this is that the surrounding media of a surface mounted antenna can be shrunk down reasonably close to the antenna. In the case of the antenna with HIGP border here, the surrounding metal surface is separated from the antenna by at most the diameter of the largest hexagonal patch that comprises the HIGP, 480 mils or 0.48 inches. This is a marked

improvement over the normal one to two wavelengths of dielectric that are required for a typical patch in a surface mounted environment.

The antenna with a PEC border did not radiate well at all. This is because the proximity of the surrounding metal border tended to short out the signal from the feed, instead of radiating. It was found, though, that the antenna with the PEC border did radiate slightly better than an isotropic radiator over several small bands. This seems counterintuitive, since, at the frequency range of operation (2–14 GHz) the gap between the antenna and the surrounding metal border would have appeared as continuous metal, making the antenna appear as a large metal plate separated from a ground plane by a layer of dielectric. It is possible that the antenna with PEC border and even the antenna with HIGP border are acting as leaky parallel plate waveguides over certain bands. A 10 mil gap is no more than $.0085\lambda$ at frequencies as high as 10 GHz. It is not likely that most of the radiation comes from the gaps between the antenna and the PEC border, or even from the gaps between the antenna and the HIGP structure. It is possible that these two structures radiate parallel plate modes that are excited from the probe-feed at the center and travel outward to the edges of the dielectric/metal plates. In the next chapter, the computational analysis that was performed provides insight as to how these structures radiate.

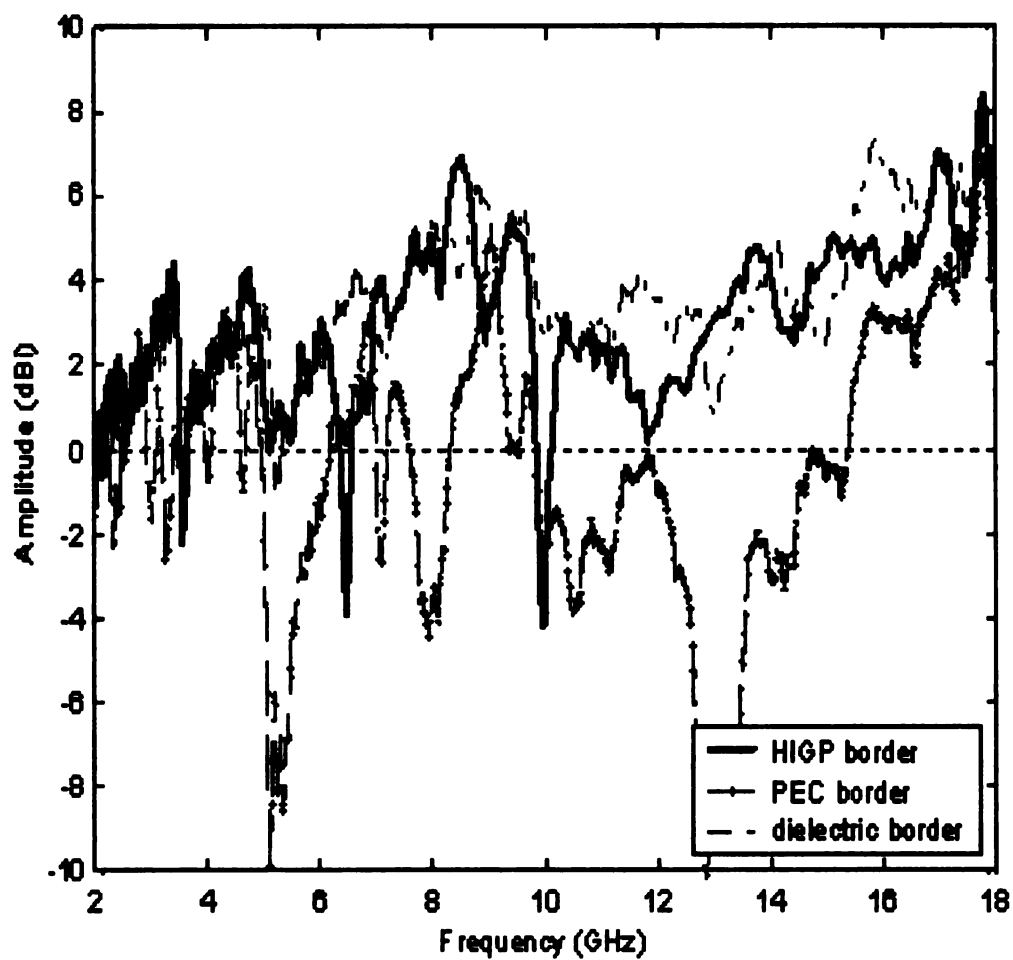


Figure 2-22: Broadside Transmission Measurement of Hexagonal Based Wideband antennas with three different borders (from [4])

2.6 Summary

This chapter has provided the background work on photonic band gap structures and high impedance ground planes. In summary, the work in this field started with extremely small structures with antennas that radiate at small wavelengths. Sievenpiper used an effective medium model to analyze structures that are small compared to a wavelength and therefore developed the surface impedance analysis of photonic band gap structures, leading to the development of high impedance ground planes. Golla, amongst others, created antenna/HIGP hybrid structures in an attempt to make surface mounted antennas smaller in surface area and in depth. Golla primarily used patch (aperture) antennas for the work he performed in this field. However, it was demonstrated in this chapter how both aperture and real source antennas can be placed very near the HIGP surface and still radiate well. The large bandwidths and relatively high gain of electric-type (real-source) antennas make them suitable for many applications, but generally not for low-profile surface mounted environments, where the depth and surface area of the antenna are a premium. That is why patch antennas are generally used, and much effort has been devoted to creating more broadband and high gain patch antennas. It would be extremely useful if the low profile of a patch could be married to the performance of electric-type antennas, a dipole for example.

The purpose of the next chapter is to provide computational analysis for the patch antennas with the three different borders that were built by Golla: the patch with dielectric, HIGP and metal borders. Because these antennas are narrow-band by nature, the results of the proceeding analysis underscore the need to use a wider-band antenna if

wide-band performance is required of the antenna/HIGP structure. This impetus leads to chapter four, where a wideband antenna is used integrally with a HIGP substrate in a four-layer design concept. This concept both improves the performance of low-profile surface-mounted antennas and permits the operation of electric-type antennas, which are known to have broader operational bandwidths, close to the ground plane that shields them.

CHAPTER 3

COMPUTATIONAL RESULTS OF PREVIOUSLY BUILT STRUCTURES

3.1 Method of analysis

The finite element method was used to simulate all structures. The particular code used herein is a Fortran77 program called *Prism* [5]. It is an edge-based FEM code with extruded triangles as the basic elements. A two dimensional structure meshed with triangular sub-elements is input into the program, and when the triangles on the two-dimensional surface are extruded three-dimensionally down multiple layers, they become prisms. The user inputs the two dimensional surface to the program, and then specifies how the surface varies layer by layer in the z-direction. A z-directed edge is then selected to be the feed edge, and a reference source field is placed upon that edge. The program then iteratively solves a Finite Element-Boundary Integral (FE - BI) matrix for the electric field coefficients on each unknown edge (non-metal edges), and then applies a near-to-far-field transformation in the form of the dyadic Green's function to obtain the far zone fields. The program can output the antenna pattern, input impedance and S-parameters at the feed, amongst other characteristics. For this analysis, the input impedance and far-field gain of the antenna were used as the main criteria as to whether a structure operates efficiently or not. In general, an antenna with an input impedance whose real part is large and imaginary part is small is a resonant structure. Matching the antenna to a typical $50\ \Omega$ transmission was not a concern, since this work focuses only on creating theoretical resonant radiating structures.

The process by which a structure is drawn in a standard drawing package and then converted into an acceptable format for the analysis code is quite lengthy and involved. For brevity's sake, this process will not be discussed here; however, the reader is referred to Appendix A for details. Figure 3-1 shows a sample square patch that has been meshed using triangular sub-elements. The model is drawn in two dimensions, with separate polygons drawn for all distinct regions of the antenna: dielectric border, antenna, and feed region. A meshing program entitled *Skymesh* is then used to produce the triangular mesh, given the coordinates of the distinct regions. The mesh is then input to *Prism* where the user specifies the number of layers and what material the triangles of each layer are made of: dielectric, metal or absorber. For this example, the sub-elements of the outer region would consist of horizontal edges made of dielectric on the top layer, and the vertical edges would be also be made of dielectric, representing the dielectric substrate surrounding and lying beneath the antenna. The metal regions, regions 2 and 3, would have horizontal edges made of metal on the top layer, and have vertical edges made of dielectric, representing the dielectric substrate. Region 3 is meshed heavily in order to have more control over which vertical edge to feed. It is important to remember that the mesh does not vary in cross section layer by layer. This can be a constraint in some cases, especially in the case of the HIGP analysis. The only parameter that changes layer by layer is the material code for each closed region and the material code for each layer, and thus for the sub-elements that comprise that region. Therefore, a square patch antenna could not be simulated over a hexagonal HIGP substrate, unless the spatial resolution of HIGP elements was high enough to where multiple elements could be flagged as antenna

elements on the top, including the dielectric space between elements, and then as HIGP elements on the next layer.

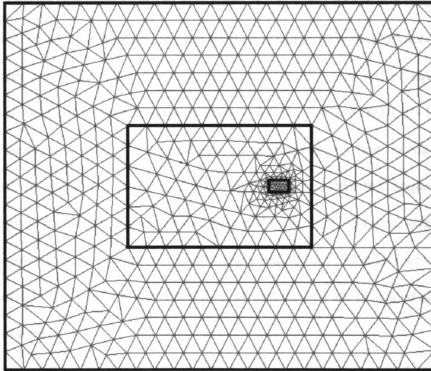


Figure 3-1: A sample finite element model of a square patch

In general, all meshes must satisfy the requirement that no edge-length is greater than $\lambda/15$ to $\lambda/20$ at the highest frequency. This requirement subsequently leads to very large meshes for structures that are electrically large (greater than 2λ on a side). For some of the structures analyzed in this work, the mesh consisted of as many as 8700 unknowns, which in a square matrix results in around 76×10^6 complex double precision memory locations. The computers used are two Linux workstations, each with four 512 MHz

parallel processors and 2 gigabytes of RAM. The most complex structures took up to eight to ten hours per frequency point using a single processor, and in order to get sufficient resolution, the structures were all tested at frequency increments of 20 MHz. Because of the available multiple processors, the frequency sweeps were divided into multiple ranges so that more than one frequency sweep could be run at a time on each machine. The structures simulated at each frequency range were meshed according to the highest frequency of that range. For example, a structure that required a frequency sweep of 2-14 GHz would have been run in 6 sweeps: 2-4 GHz, 4-6, 6-8, 8-10, 10-12, and 12-14 GHz with the mesh of each sweep range becoming progressively finer in edge-size resolution as the frequency increases. Even with this ability, some full frequency sweeps took as long as four weeks. The structures built and tested by Golla were swept from 2-18 GHz. The computers used to analyze them simply did not have enough memory to feasibly simulate this whole range. Therefore, all simulations are truncated at 14 GHz, and some to 8 GHz.

The *Prism* program is a versatile and robust code, and has shown good agreement between computational results and experimental data for virtually any finite planar electromagnetic surface. For a more detailed discussion of the *Prism* program, the reader is referred to Chapter 3 of [12].

3.2 Wideband Hexagonal Patch with Normal Dielectric Border

The first patch simulated, shown in Figure 2-19, is the wideband hexagonal-based patch antenna that Golla designed, built and measured. The actual mesh used to represent the structure from 2-4 GHz is shown in Figure 3-2. This antenna was simulated from 2-14 GHz in increments of 20 MHz. The input impedance is shown in Figure 3-3. From the computational analysis, it appears that the patch is very narrowband. The antenna was then simulated at 4.4186 GHz in order to obtain information about the surface fields at this particular frequency. From Figure 3-3, 4.4186 GHz is the first frequency at which the real part of the input impedance is non-zero and the imaginary part goes through zero. There are other frequencies at which the reactive input impedance goes through zero. However, the real part equals zero at many of these points. The data collected at the single resonant point is in the form of electric field coefficients for each finite-element edge of the mesh. The data was then imported and plotted in Matlab. The results of this single-frequency simulation are shown in Figure 3-4. The total tangential surface fields are shown in (a) and the z-directed surface fields are shown in (b). The highest intensity of field strength is located near the feed point for both field polarizations. The tangential fields are necessarily zero under the metal patch to satisfy the boundary conditions. Upon further inspection, it can be seen that the z-directed fields have large magnitudes out away from the patch, only roughly 1 to 2 db down from the maximum value at the feed, indicating the presence of traveling surface waves.

The input impedance, from Figure 3-3, goes through second much smaller resonance at 6.2685 GHz. The surface fields of the antenna were collected at this frequency as well,

in order to determine whether different parts of the antenna were indeed radiating at different frequencies. The results of this simulation are shown in Figure 3-5.

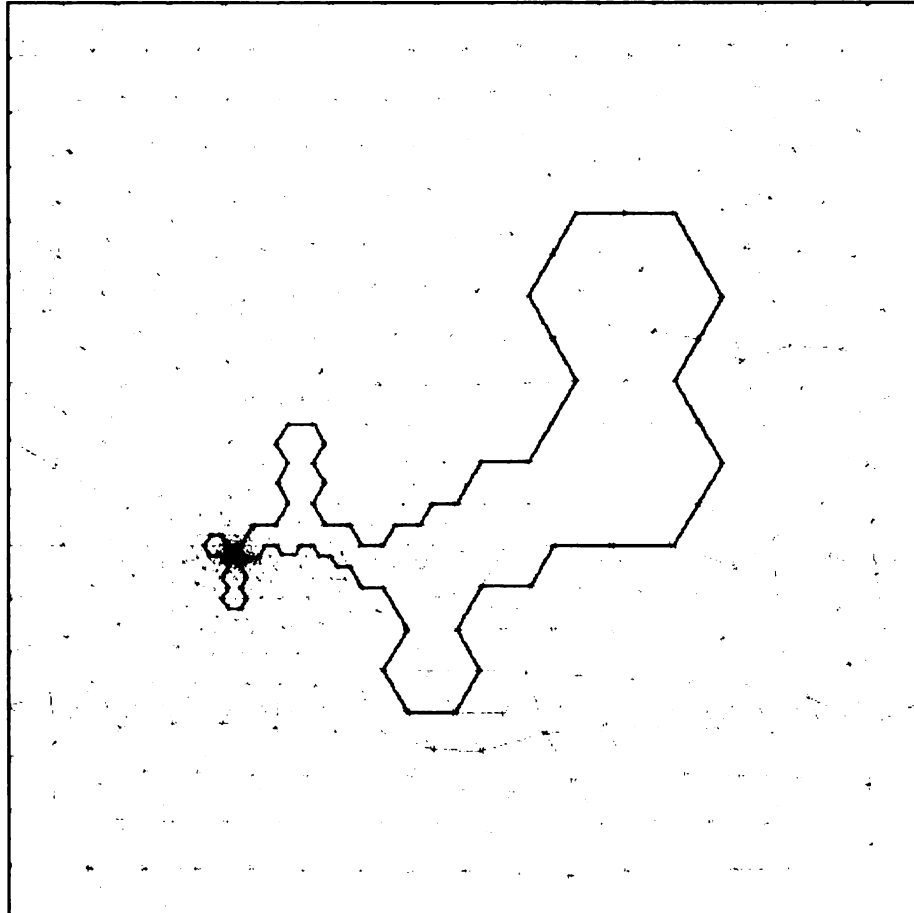


Figure 3-2: Sample Mesh for Wideband Patch used from 2-4 GHz

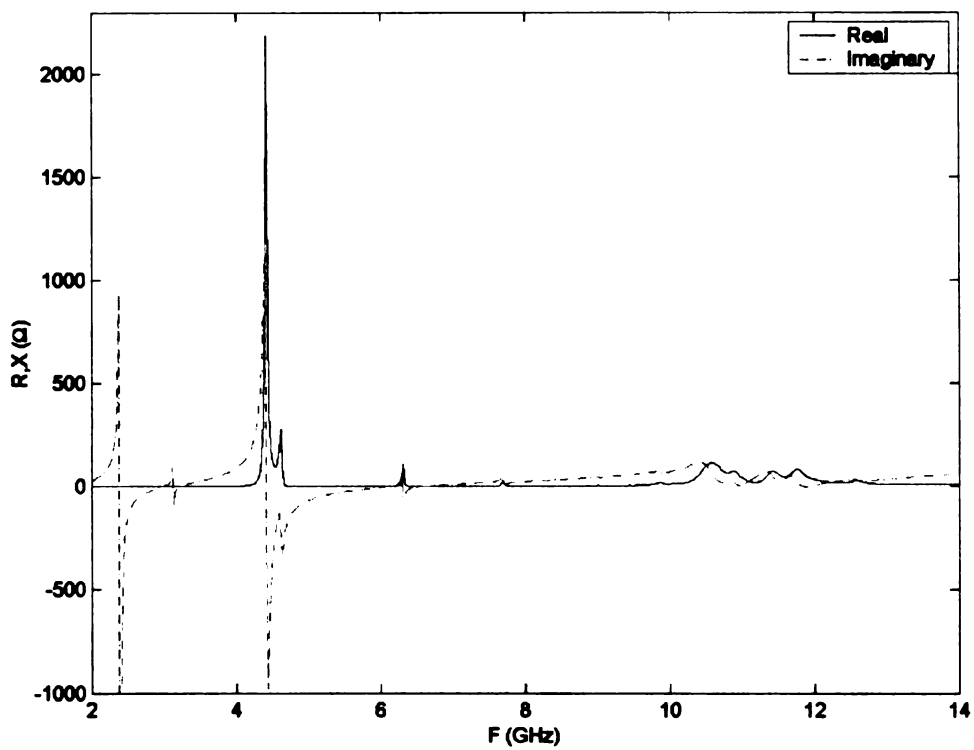
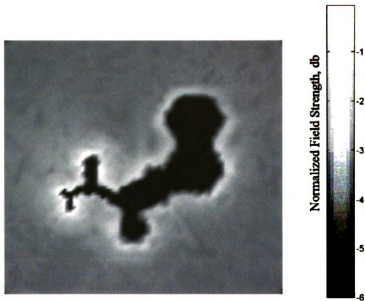
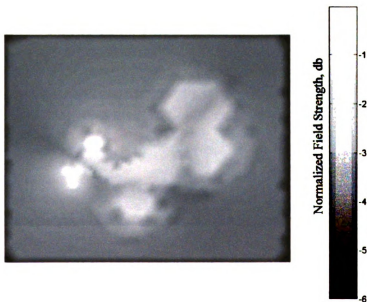


Figure 3-3: Input Impedance of Wideband Hexagonal-based Patch with simple Dielectric Border

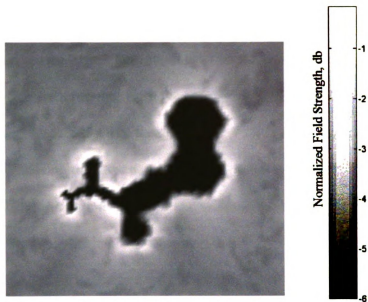


(a)

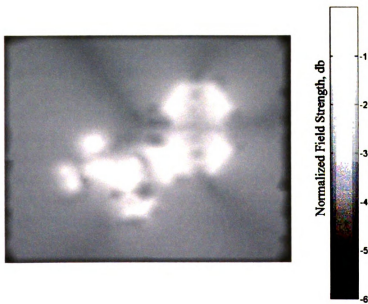


(b)

Figure 3-4: Normalized tangential (a) and z-directed (b) substrate-level E-field strength for hex-based wideband patch antenna at 4.4186 GHz



(a)



(b)

Figure 3-5: Normalized tangential (a) and z-directed (b) substrate-level E-field strength for hex-based wideband patch antenna at 6.2685 GHz

It can be seen, upon comparing the normal z-directed surface fields at 4.4186 and 6.2685 GHz that the antenna certainly does radiate more at different places for different frequencies. On the two largest hexagonal pads on the right side of the antenna, at 4.4186 GHz there is a clear null running from the top of the upper pad to the bottom of the lower pad in a wide arc. At 6.2685 GHz, there are now two nulls in this vicinity, perpendicular to each other, indicating the presence of a different radiating mode. There is clearly more relative energy at this location on the antenna than at the lower resonance.

The design principle behind this antenna is that if a wideband patch antenna can be created, then it would be useful to create a wideband HIGP surface to fit around it. The next section discusses computational results from the wideband patch and the wideband HIGP border.

3.3 Wideband Patch with HIGP Border

The wideband hexagonal-based patch with a high-impedance ground plane border (Figure 2-20) that was built and tested by Golla was also simulated and analyzed computationally. The actual mesh used for this structure is shown in Figure 3-6. Because of the extremely small air gaps (10 mils) separating the antenna from the HIGP elements, and the HIGP elements themselves, the meshing program, *SkyMesh*, must create triangles with extremely small edge-lengths in order to accurately represent the structure. At 14 GHz, the number of triangular sub-elements in the mesh that represents the antenna with the HIGP border is seven times that of the mesh that represents only the patch, (Figure 3-2). Because of the extremely high number of unknowns, and the huge matrices that are created when the FEM program solves for the fields, it was necessary to truncate the frequency sweep at 8 GHz. Meshing at higher frequencies simply required too much memory and computation time. In order to sweep to 8 GHz, the computers ran four sub-sweeps in 2 GHz increments for a total raw computation time of about five weeks. Further simulations would have taken even longer because of the increased resolution in mesh size at the higher frequencies. The mesh was therefore swept from 2-8 GHz in increments of .02 GHz. The input impedance is shown in Figure 3-7.

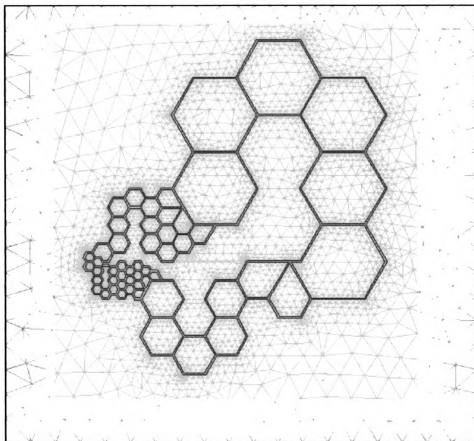


Figure 3-6: Mesh used for Wideband Patch with HIGP border from 2-4 GHz

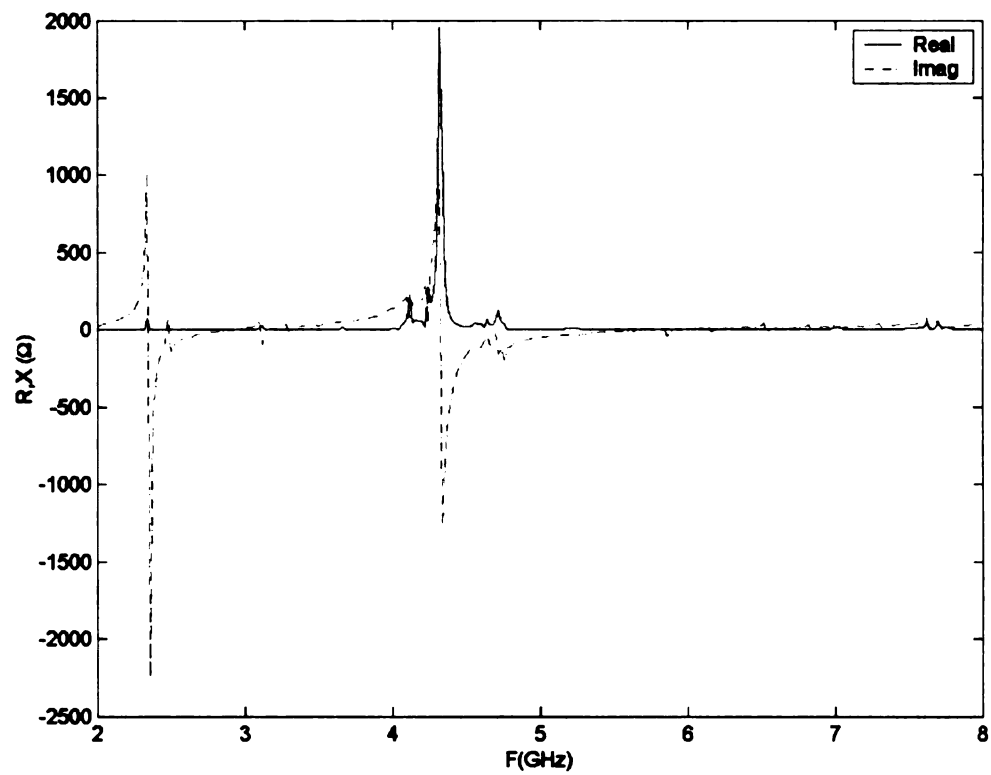
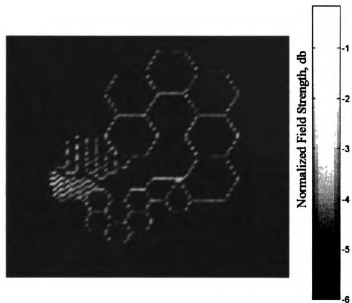
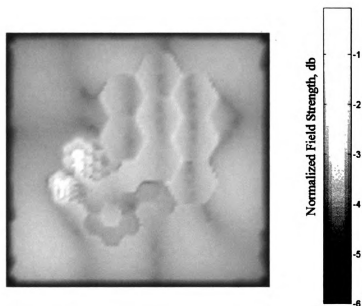


Figure 3-7: Input Impedance for Wideband Patch with HIGP border

Above 5 GHz, the antenna is a short circuit. It is likely that truncating the frequency sweeps at 8 GHz caused no loss in useful data. There appears to be only one resonant frequency for this structure, at 4.32645 GHz. From the computational analysis, the antenna with HIGP is as narrow band as the antenna by itself. The antenna was simulated at the resonant frequency and the surface fields were again collected and plotted. The normalized tangential and z-directed fields are shown in Figure 3-8 (a) and (b) respectively. Because the border is mostly PEC, the tangential surface fields are zero throughout most of the structure except for inside the air gaps. It can also be seen that the tangential fields in the gaps are higher in intensity in the gaps that are closer to the feed region, and much lower in intensity in the gaps that are away from the feed region. The normal surface fields, however, are intense even away from the feed region. It is possible that these fields move outward radially toward the edges of the structure, as in a parallel plate waveguide, and radiate from the edges.



(a)



(b)

Figure 3-8: Normalized Tangential (a) and Z-directed (b) Substrate-Level E-field Strength for Wideband Patch with HIGP Border at 4.32645 GHz

3.4 Wideband Patch with PEC border

The final structure simulated is the wideband patch with the PEC border that runs directly up to the edge of the antenna, with only a 10 mil gap separating the antenna from the PEC border. The input impedance for this antenna is shown in Figure 3-9. This antenna was simulated from 2-14 GHz in .02 GHz increments. The real part of the input impedance is zero or very near zero across the entire frequency range. This is not surprising, since across the entire frequency range, the antenna most certainly appears to be a large metal plate above a ground plane separated by a layer of dielectric with a vertical probe feed in between. Surface fields were not collected and plotted for this structure since the antenna does not resonate in this band.

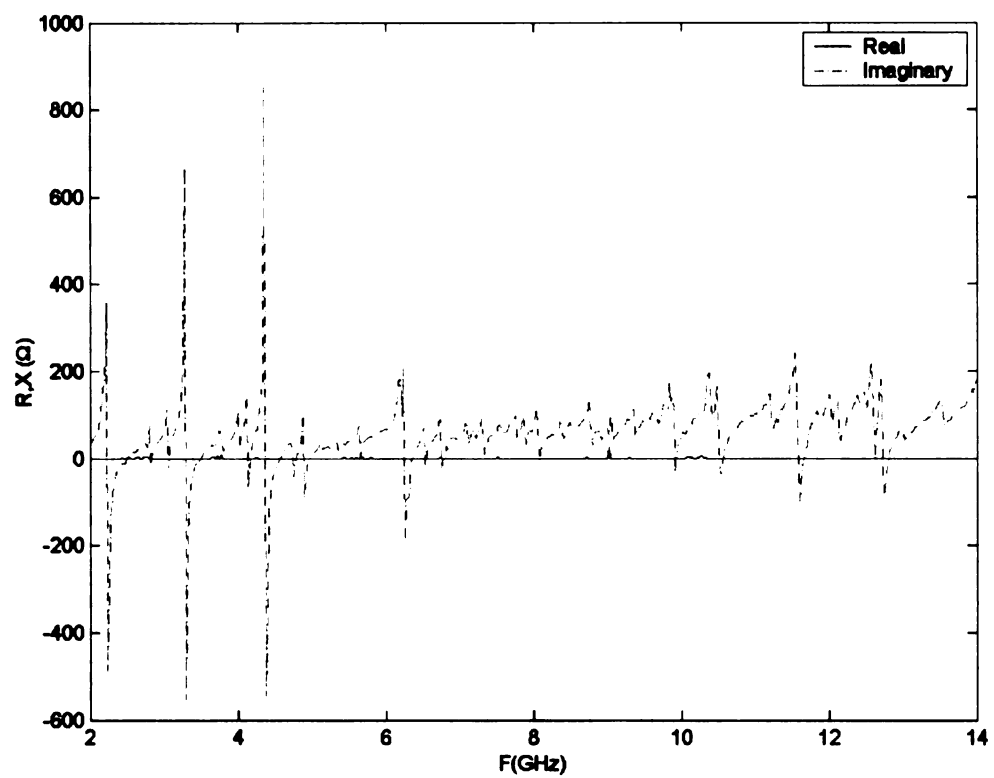


Figure 3-9: Input Impedance for the Wideband Patch with PEC Border

3.5 Conclusions

The structures simulated here have one problem in common: they are very narrow band. Even the patch by itself only resonates at two distinct frequencies, and away from those frequencies, the real part of the input impedance goes to zero. Consequently, the antenna with the HIGP border does not perform much better, since it is based on the same antenna.

The new design work at MSU focused on starting with a known broadband antenna and building a HIGP surface to fit to it. This antenna takes the form of the printed bowtie dipole. The next chapter discusses the design principles used for this antenna and the HIGP surface for it, as well as computational results.

CHAPTER 4

PROPOSED FOUR LAYER ANTENNA/HIGP DESIGN METHOD

4.1 Introduction

Part of Golla's work involved taking copper-tape monopoles and placing them flat against a HIGP surface. His theory was that since the HIGP is known to reflect incident electric fields in the PBG of the surface in phase, if a monopole antenna was placed directly adjacent (touching) a HIGP surface, the surface should reflect the incident wave in phase and will thereby allow the antenna to radiate as a monopole. Golla found that this structure did not work well. However, placing the antenna directly on the HIGP surface most likely shorted the antenna to ground through the vias. This structure may operate quite a bit more efficiently if a small gap is placed between the antenna and the HIGP surface. The design work done at MSU focused on extending Golla's work with electric source antennas to multi-layer antenna/HIGP combinations that make use of the zero-reflected-phase property of the HIGP.

The designs presented in this chapter all use a dipole separated from the HIGP surface or the ground plane underneath with a thin layer of substrate. A bowtie dipole is the antenna chosen, because of its known broadband characteristics. When a printed bowtie dipole is placed parallel in close proximity to a ground plane, it behaves like a two-element array of triangular patches. However, when the same antenna is placed parallel in close proximity to a HIGP surface with a thin slab of dielectric separating the two, the antenna starts to behave like a normal dipole. It must be reiterated that the designs in this

section are not completely optimized. They do, however, underscore two important points. First, a wideband dipole antenna can be placed very close to the ground plane that shields it in the backward half-space and still exhibit characteristics that are typical of a dipole: strong radiation in the plane parallel to the dipole axis and decent impedance matching over a significant bandwidth compared to a patch antenna. Second, this section shows that the periodicity of HIGP elements does not necessarily have to be much smaller than the wavelength of operation, i.e., the ratio of HIGP elements to the wavelength of operation does not have to be in the vicinity of 20:1 or thereabouts, as previously thought. The new structures proposed here and the design concept introduced permit decent operation from a bowtie dipole with a periodicity as low as 4:1, four HIGP elements per wavelength of operation. Though not optimized and perfectly matched to 50 Ω transmission lines, this work opens a new door in HIGP/antenna hybrid structures.

4.2 Bowtie Dipole over HIGP Substrate

Figure 4-1 shows the top view of a bowtie dipole with a HIGP substrate.

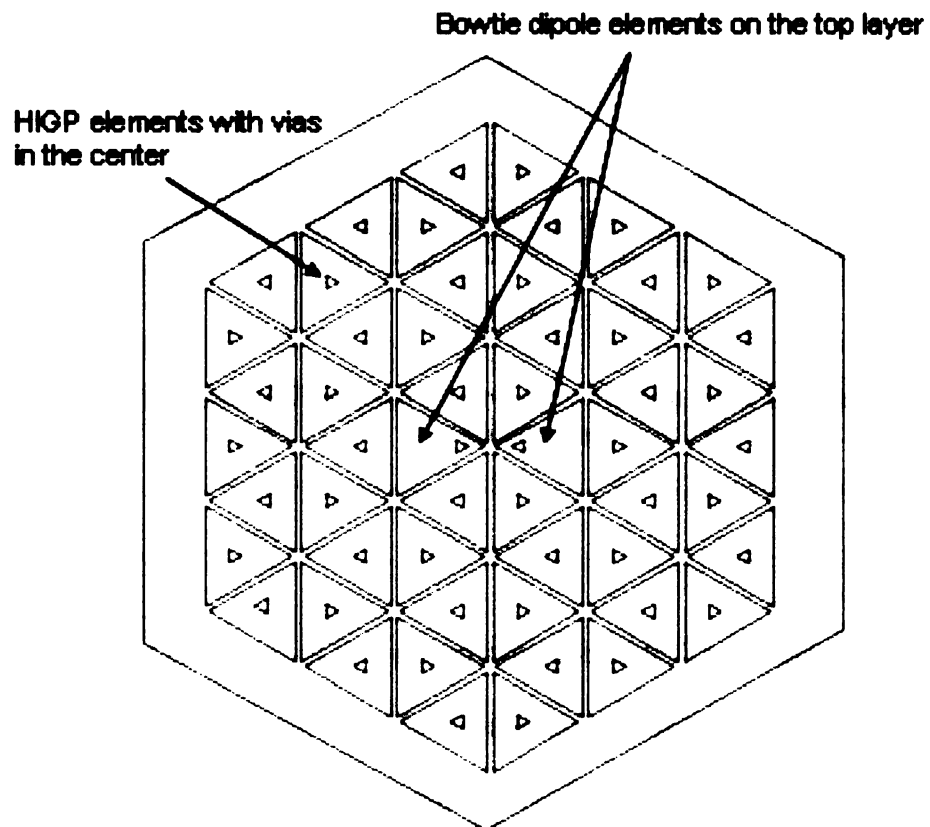


Figure 4-1: A Bowtie Antenna with HIGP Substrate

A cross-sectional view of this structure is seen in Figure 4-2. These figures represent the four-layer design method for combining dipole antennas with HIGP substrates.

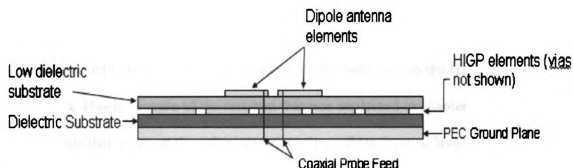


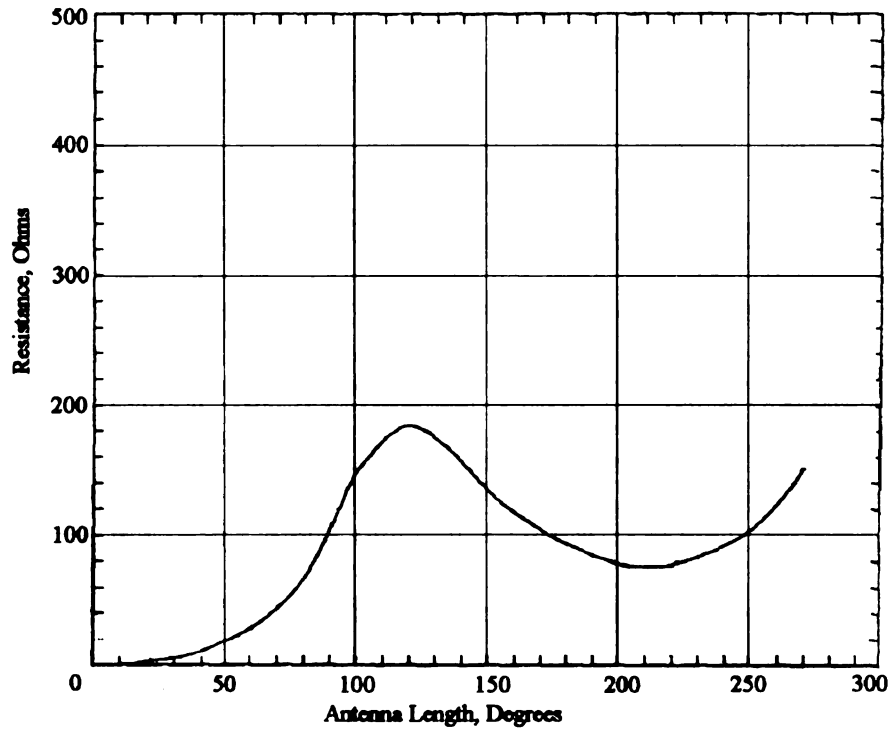
Figure 4-2: Cross Section of Proposed Four-Layer Design for a Dipole over a HIGP Substrate

The dipole is printed on a layer of low-permittivity substrate. The substrate is then placed directly on top of the HIGP elements, which have been printed on a layer of grounded dielectric substrate. This design concept takes advantage of the zero-reflection phase property of the HIGP, in that a real-source antenna is placed above the HIGP and can still operate regardless of its proximity to the metal HIGP elements. The antenna feed is simulated via a probe that exists on one of the vertical dielectric edges immediately under the antenna. In reality, this feed could be accomplished by aligning the vias of the HIGP elements with the antenna and running the center conductor of a coax up through one of the vias, and attaching the outer conductor to the ground plane underneath. The two

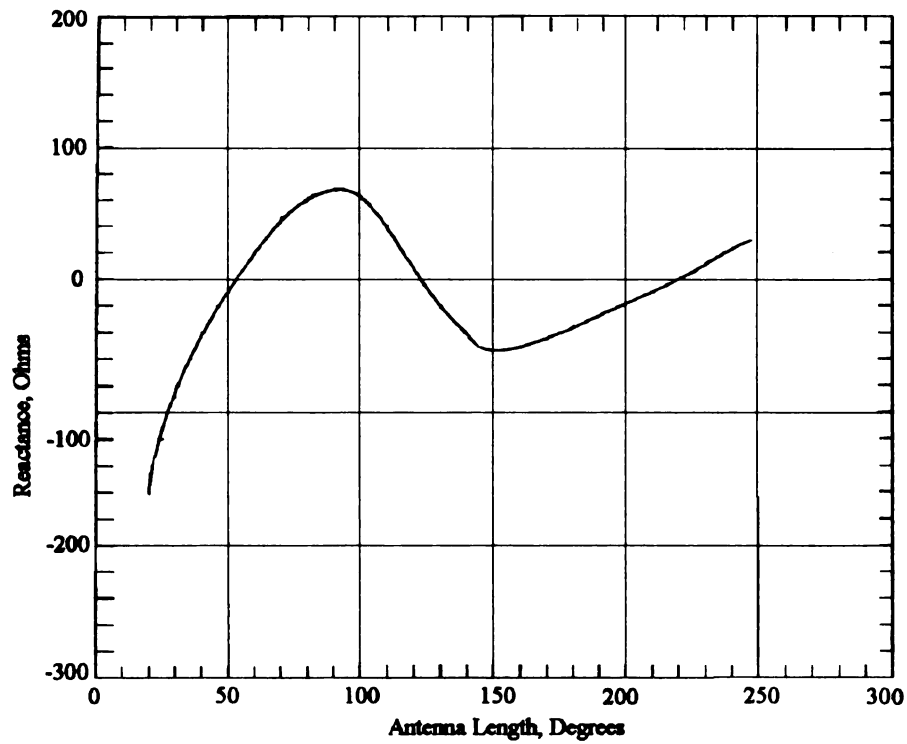
simulated probe feeds have unity voltage strength with 180° of phase shift between the two probes, the so-called “push-pull” feed arrangement. The HIGP was designed using the equations for sheet capacitance and inductance found in chapter two. The gap between elements (g) is 2.0 mm. The center-to-center spacing between vias (a) is 2.13 cm., and the edge-length of an element (w) is 3.21 cm. The substrate separating the antenna from the HIGP has a dielectric constant of 2.0 with a thickness of 59 mils (1.5 mm), and the HIGP substrate has a dielectric constant of 4.9 with a thickness of 59 mils. Each antenna half shown in Figure 4-1 is exactly the same size as the HIGP elements underneath. This is because of the restraint that was explained in chapter three, that only the materials that make up the sub-elements can vary from layer to layer, not the cross-section of the mesh. The antenna consists of prisms whose tangential edges on top are metal, and vertical edges (edges of the prism) are dielectric. All surrounding regions on the top layer consist of prisms whose tangential edges on the top layer and whose vertical edges are all dielectric. The HIGP elements, on the second layer, have metal tangential prism edges on top and vertical dielectric prism edges below to represent the layer of substrate below the HIGP elements. The small triangles in the middle of the HIGP elements represent vertical vias, whose tangential prism edges are also metal on top but whose vertical prism edges are metal instead of dielectric, connecting the HIGP to ground. The bottom tangential edges of the prisms on the second layer are metal to account for the ground plane underneath the entire structure. The HIGP substrate shown in Figure 4-1, according to the design equations of chapter 2, has a resonant frequency of 3.5 GHz. The antenna was simulated from 1 to 6 GHz in 20 MHz increments. Figure 4-3 is a plot of measured resistance and reactance curves for a triangular monopole (bowtie

monopole) of 60° flare angle over a ground plane. The antennas in this chapter all have a flare angle of 60° . According to Figure 4-3, this antenna has an electrical length of 47° at 1 GHz and 283° at 6 GHz. Electrical degrees are defined as the product of the physical length of each monopole and $360^\circ/\lambda_g$, where λ_g is the applied (guided) wavelength. Since this antenna is simulated over a substrate with permittivity of 2.0, the guided wavelength is the freespace wavelength divided by $\sqrt{2.0}$. According to Figure 4-3, at 120 electrical degrees, a bowtie dipole with 60° flare angle will encounter its first resonance. This corresponds to 8.3334 cm of guided wavelength, or 2.57 GHz. The antenna is not designed exactly to fit with the PBG of the substrate, but these are some design tradeoffs that are encountered when optimizing computation time. At the resonant frequency of the HIGP, the antenna is 165 electrical degrees in length. However, there are many design parameters to consider when performing computational analysis on these structures: the resonant frequency of the HIGP, the resonant frequency of the antenna, the periodicity of the surface vs. the guided wavelength, and the overall frequency range of operation. The first criterion was that the structure be operated at low frequencies to reduce the number of sub-elements used to represent the structure, thus reducing the overall computation time. It was found, however, that this structure still required around five weeks of computation time, even when dividing the frequency sweep into multiple ranges. A second criterion for this design is that the dielectric substrates be of commonly found materials in industry, such as FR4 or other substrates. This requirement is relaxed in other designs in order to better fit the antenna to the HIGP.

The periodicity of the HIGP elements vs. the guided wavelength is 4:1, or four HIGP elements per guided wavelength.



(a)



(b)

Figure 4-3: Measured Resistance (a) and Reactance (b) vs. Electrical Length for Triangular Dipole with 60° Flare Angle (from [13])

The computed input impedance of this antenna is shown in Figure 4-4. The antenna appears to resonate at around 3.95 GHz, off from the expected resonant value. This is perhaps due to the fact that the antenna and HIGP are not optimized together. However, an expanded view of the input impedance is shown in Figure 4-5. While not perfectly matched to a 50 Ω transmission line, the real part is certainly non-zero over a significant portion of the measurement band. If the center frequency is taken to be 3.95 GHz, then the plot of Figure 4-5 represents a fairly matched antenna over a 20% bandwidth of the center frequency. With some simple tuning methods, such as changing the location of the probe feed, the real part of the input impedance can be perfectly matched to a 50 Ω transmission line.

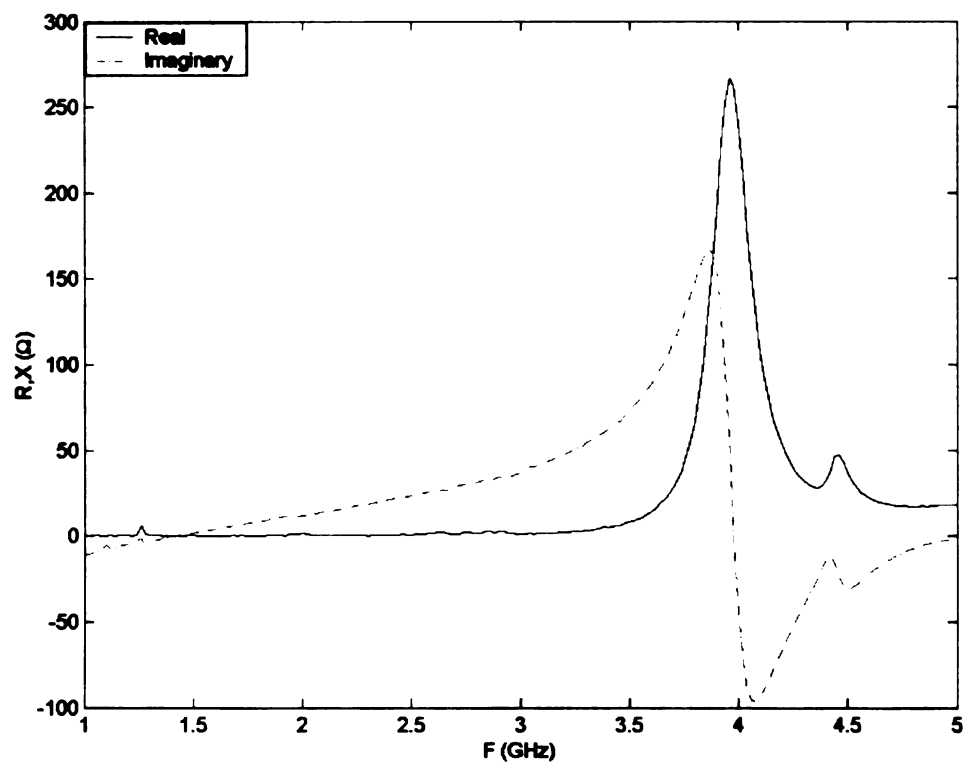


Figure 4-4: Computed Input Impedance for the Bowtie Antenna with HIGP substrate

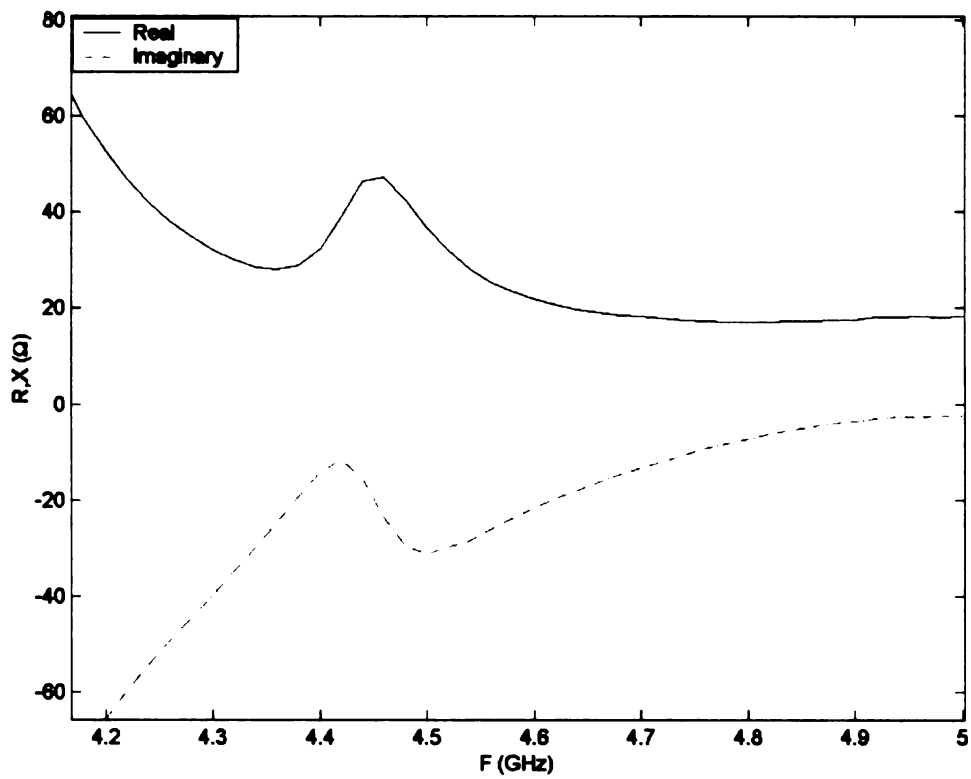


Figure 4-5: Expanded view of Input Impedance of Bowtie Dipole over HIGP substrate from 4.2 – 5GHz

One of the goals of this thesis is to determine the fewest number of elements possible to achieve HIGP performance. Even without changing the periodicity of the structure, the structure analyzed in this section can be reduced in size (and therefore matrix entry unknowns) simply by removing one ring of HIGP elements from the outside of the surface. This structure is shown in Figure 4-6. This structure now has only one ring of HIGP elements surrounding the antenna instead of two. This resulted in a reduction of computation time by a factor of one-fifth, because of the lower number of FEM elements used to represent the structure. It was found that reducing the structure did not have an effect on the input impedance, as shown in Figure 4-7. Though it is not shown here, in an expanded view of the antenna with the HIGP substrate, the input resistance settles to around 20Ω just like the substrate with one extra layer of elements. Since the extra ring of elements surrounding the HIGP surface did not affect the performance of the antenna, higher frequencies (and thus more sub-elements) could feasibly be simulated, allowing for the antenna and HIGP to be designed to resonate closely together.

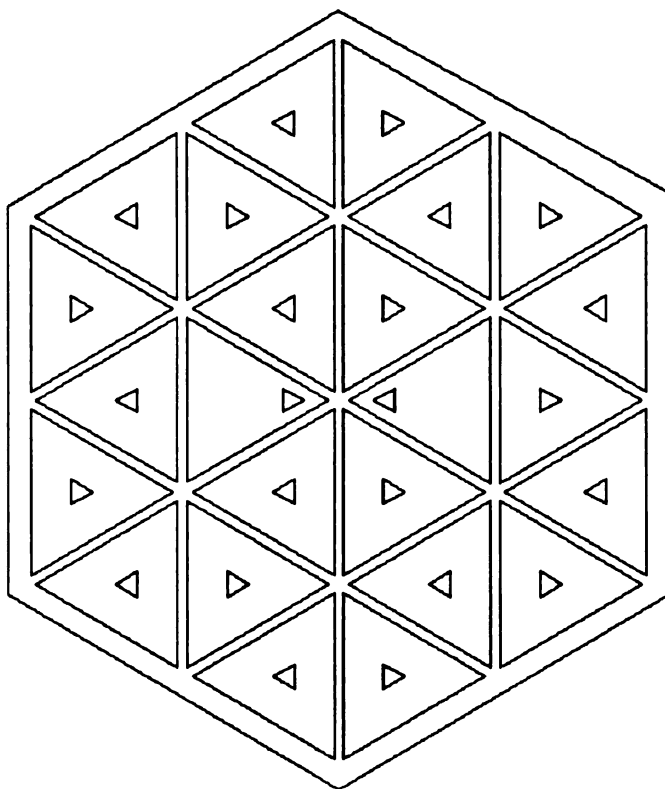


Figure 4-6: Bowtie Dipole with HIGP-Substrate with Reduced Number of Elements

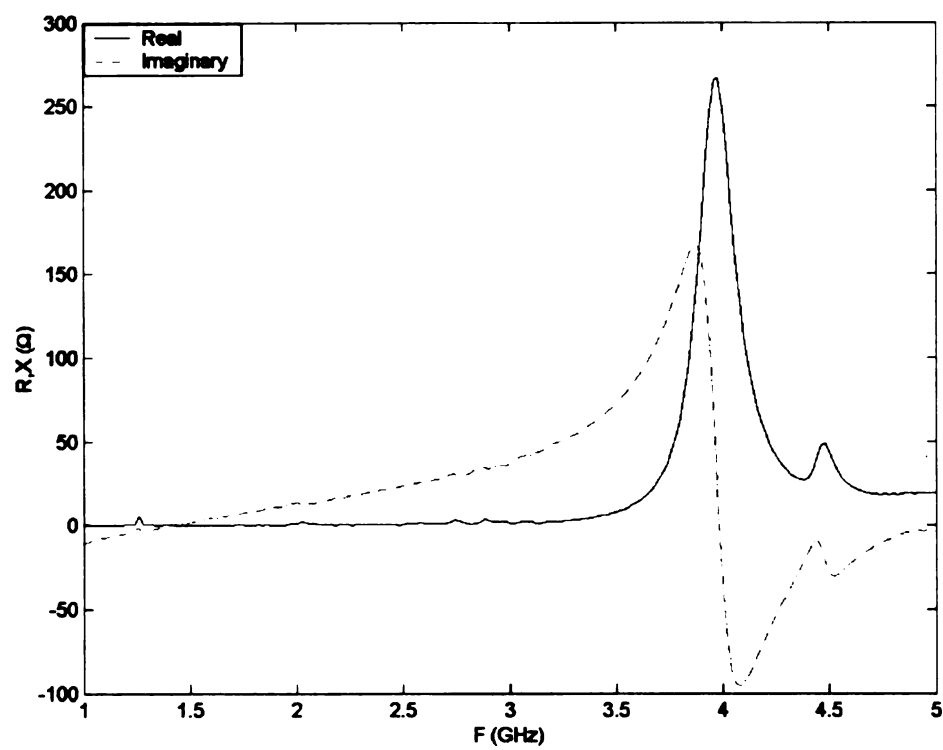


Figure 4-7: Input Impedance of Bowtie Dipole with Reduced-Size HIGP Substrate

4.3 Bowtie Dipole over Grounded Dielectric Substrate

The bowtie dipole was also simulated over a grounded dielectric substrate, as demonstrated in Figure 4-8.

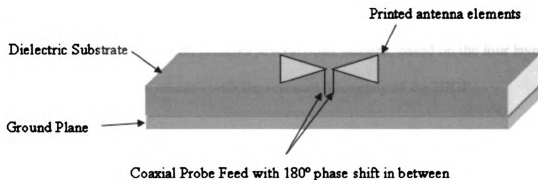


Figure 4-8: Diagram of a Printed Bowtie over Grounded Dielectric Substrate

It is expected that the antenna, when operated in this configuration, will behave as a two-element array of patches, probe-fed with a 180° phase shift between the feeds. The computed input impedance of this antenna is shown in Figure 4-9. The real part of the input impedance becomes very large at resonance. The input impedance moves quickly off resonance, however, indicating that the antenna is acting like a two-element array of patches. Figure 4-10 shows an expanded view of the input resistance of the antenna over the HIGP and grounded dielectric substrates. The input resistance of the antenna over the grounded dielectric substrate quickly moves from resonance back down to $0\ \Omega$, as is expected for a patch antenna. The input resistance of the antenna over the HIGP

substrate, though, hovers around $20\ \Omega$ over a significant band. This plot reiterates the non-patch-like behavior of the antenna over the HIGP substrate, even when the antenna and HIGP surface are not optimized together. This plot also suggests that the bandwidth of operation of the HIGP spans several GHz. Since the antennas with the two different substrates both appear to resonate at the same frequency, it can be inferred that the antenna with HIGP substrate acts as a patch at the resonance shown here. But away from the patch resonance, the dipole radiation mode takes over, still within the PBG of the HIGP substrate. The next section presents several other designs, based on the four layer concept, that optimize the antenna with the resonant frequency of the HIGP.

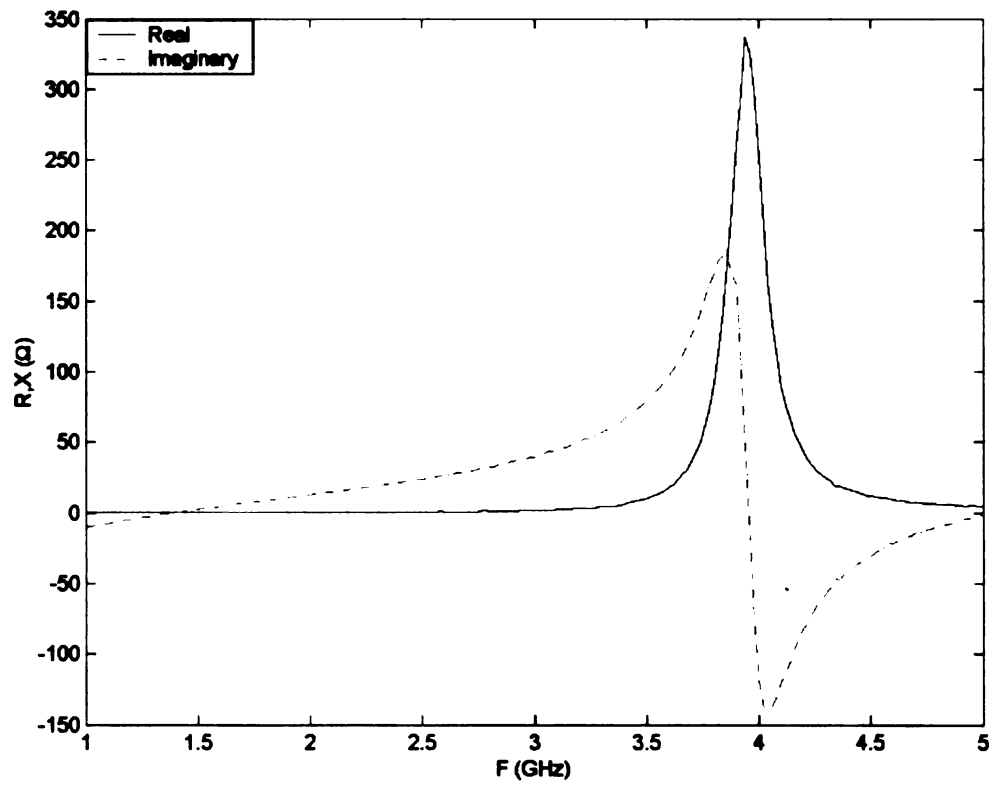


Figure 4-9: Input Impedance of a Probe-fed Bowtie Antenna over Grounded Dielectric Substrate

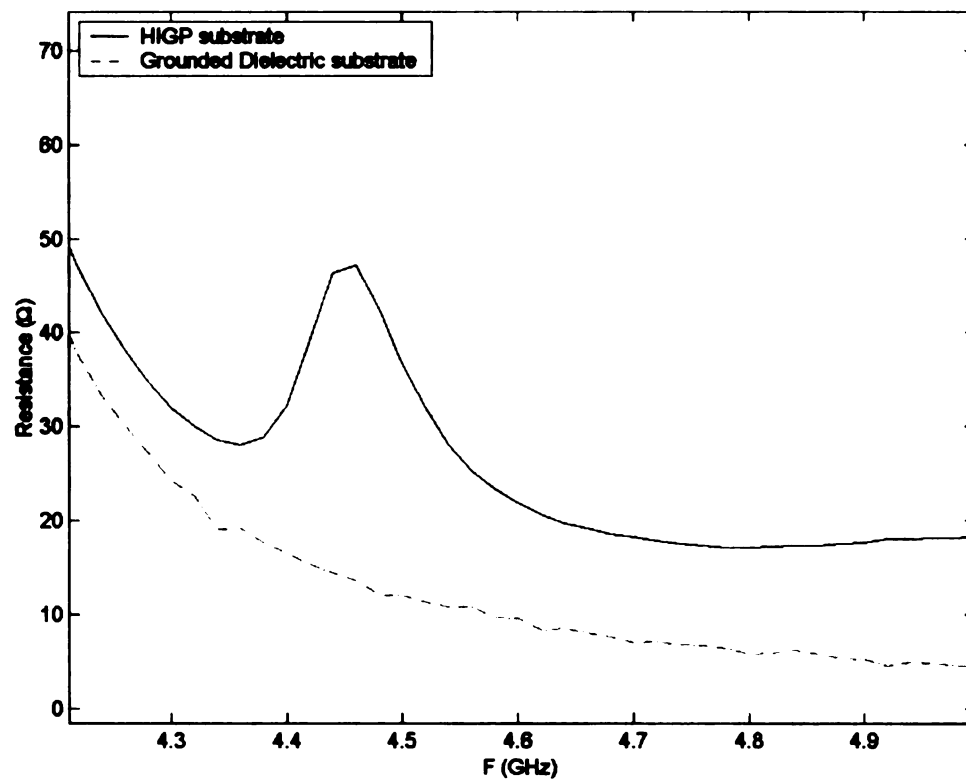


Figure 4-10: Expanded Input Resistance of the Bowtie over HIGP and Grounded Dielectric Substrate from 4.2 – 5.0 GHz

4.4 Optimized Bowtie Dipole/HIGP Design

A design for a HIGP/Bowtie antenna combination that brings the resonant frequency of the antenna closer to the resonant frequency of the HIGP is now presented. A further criterion for this optimized design is that the periodicity of the HIGP surface be increased to 5:1, or five HIGP elements per guided wavelength at resonance. This required tailoring the size and spacing of the elements as well as the materials on which the structure is built. The basic shape of the structure is relatively identical to the one analyzed in the previous section, simply the size of the elements and their spacing has changed. For this reason, a picture of the optimized design is not provided.

The optimized design has elements spaced 1.0 mm from each other, with an edge length of 1.675 cm. and a center-to-center via spacing of 1.1 cm. The dielectric substrate underneath the elements is 59 mils in thickness with a dielectric constant of 4.9. However, the substrate separating the antenna from the HIGP layer is a 'custom designed' material, with a dielectric constant of 1.23 and a thickness of 59 mils. This makes the resonant frequency of the HIGP 5.1 GHz. The antenna is now roughly 100 degrees in electrical length at the resonant frequency of the HIGP. Furthermore, the element periodicity is now 5:1 at resonance, or 5 HIGP elements per wavelength. This structure was simulated from 4 GHz to 6 GHz. The antenna was then simulated over a grounded dielectric substrate, to compare the operation of the two substrates. The input resistance of the antenna with these two substrates is shown in Figure 4-11. The first noticeable characteristic about this plot is that the input resistance (R_{in}) of the antenna over HIGP substrate is higher than the R_{in} of the antenna over grounded dielectric

substrate over almost a 1.4 GHz band. While the actual value of resistance is not high, the R_{in} can be tuned to $50\ \Omega$ by moving the probe feed around on the antenna. It is left for future investigation to perform this investigation. Furthermore, the spacing of the two dipole halves is 5 mm. This parameter is not flexible, based on the drawing of the HIGP structure underneath and the constraint mentioned previously about the cross-section of the layers not changing from layer to layer. The dipole feed gap could play a large part in the value of the input impedance. If the dipole halves are spaced too far apart, the input resistance of the antenna drops.

There are two distinct peaks in the input resistance, indicating that either the antenna or the HIGP operates in a multi-mode fashion. Also of interest is the clear lack of a distinct resonant peak, as was found in the first design presented. It is believed that the first design operated more like a resonant patch over HIGP substrate because the antenna and HIGP were not optimized together. However, it is believed that this antenna is operating as a pure dipole, albeit not a well matched one, but still utilizing the zero-reflection phase property of the HIGP nonetheless. Furthermore, this behavior is seen even when the periodicity of the HIGP is as low as 5:1. Were the periodicity increased to 10:1 or greater, perhaps distinct dipole resonant behavior would be observed. The huge number of sub-elements required to simulate such a structure renders this task unfeasible with the analysis method used here. However, use of a mixed-element (hexahedral/prism) FEM code offers the promise of accomplishing this analysis due to the reduced number of aperture unknowns using that method. Such a tool is currently being developed at Michigan State University.

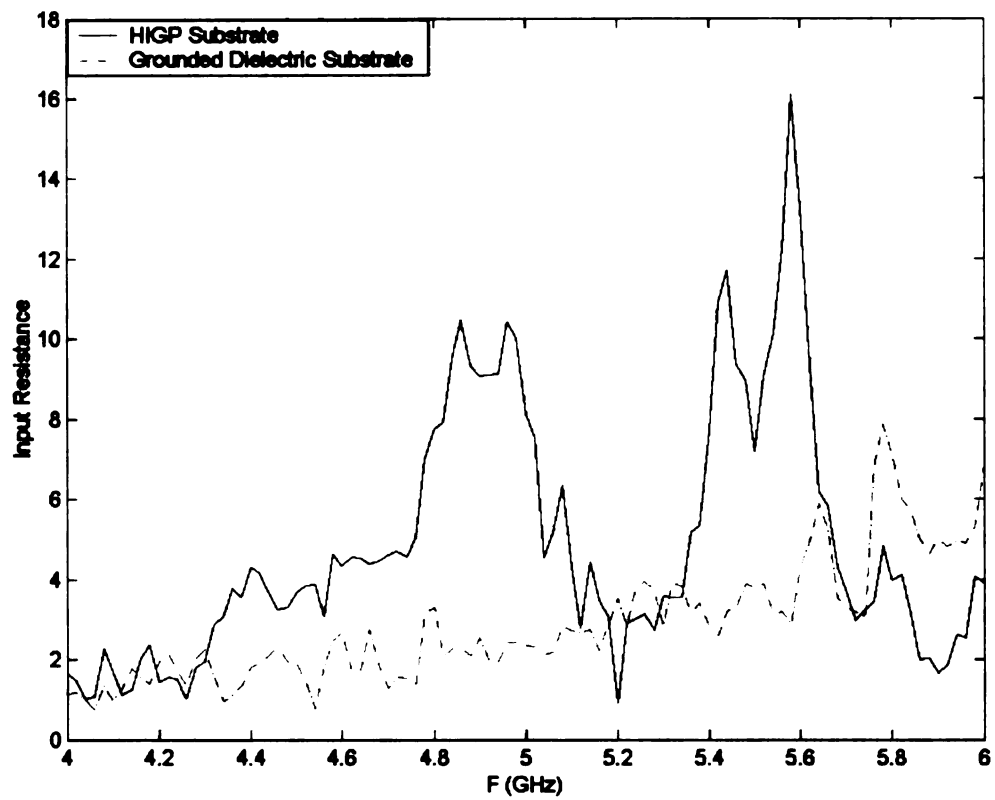


Figure 4-11: Input Resistance for Bowtie Antenna over HIGP and Grounded Dielectric Substrates

Figure 4-12 and Figure 4-13 show the broadside normalized E-plane and H-plane gain vs. incident angle for the bowtie over the two substrates. In the E-plane pattern cut, the dipole halves are oriented along the y-axis, and the measurement is taken with $\phi = 90^\circ$, aligned with the y-axis and θ is swept from -90° to 90° . The fields plotted are θ -directed fields. The H-plane pattern cut is taken with the same orientation but with $\phi = 0^\circ$, aligned with the x-axis. The frequency is 5.58 GHz, corresponding to the largest value of resistive input impedance from Figure 4-11. The gain of the antenna over the HIGP substrate in the E-plane is a full 10 db greater than that of the dielectric substrate over 120° of the coverage area. The offset null at 30° is most likely attributable to either under-meshing (under-sampling) or having an asymmetry near the feed region in the mesh that is used to simulate the structure, or by the large gap separation in the dipole halves. Furthermore, an ideal dipole has an expected null at grazing angles of incidence, here towards $\theta = -90^\circ$ and 90° . However, the pattern is still strong at these angles. This suggests that the HIGP substrate is not suppressing surface fields as it is expected to do. Figure 4-14 and Figure 4-15 show the normalized tangential and z-directed electric fields for the antenna over the two substrates. While the electric field intensity is certainly lower for both field polarizations towards the edges with the HIGP substrate compared to the dielectric substrate, there is most likely enough energy to contribute to significant gain at grazing angles of incidence or transmission.

A nearly omni-directional pattern is expected in the H-plane pattern of the antenna over HIGP substrate, since the H-plane fields of a dipole do not vary when the measurement is broadside. Again, this is most likely attributable to imperfections in the mesh. The antenna over the dielectric substrate simply behaves like a patch off resonance. A distinct

nearly omni-directional pattern is observed in both principal plane cuts for the antenna over grounded substrate.

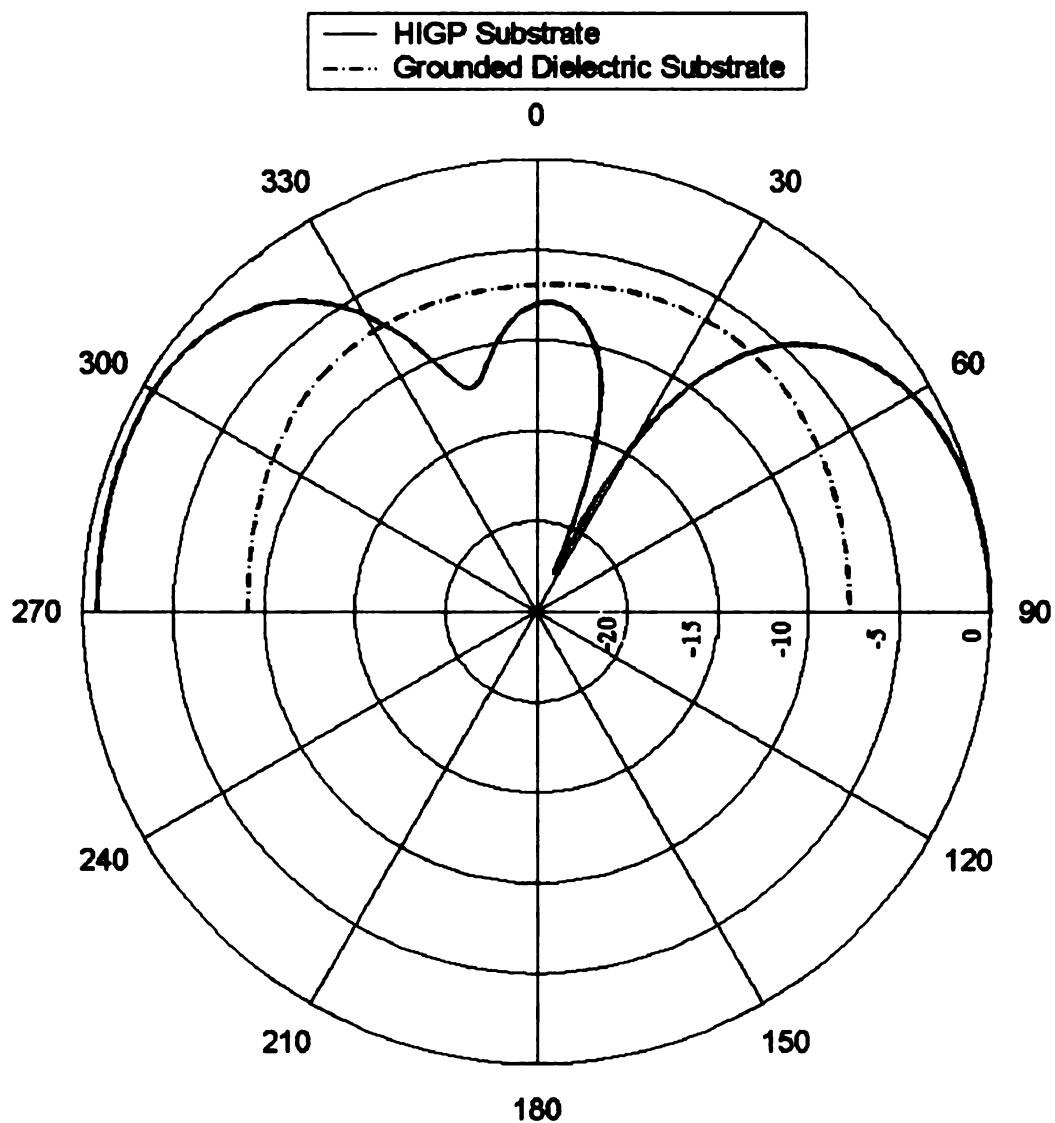


Figure 4-12: Broadside Normalized E-plane Pattern (gain, db) of the Bowtie Antenna with HIGP Substrate and Grounded Dielectric Substrate, F=5.58 GHz

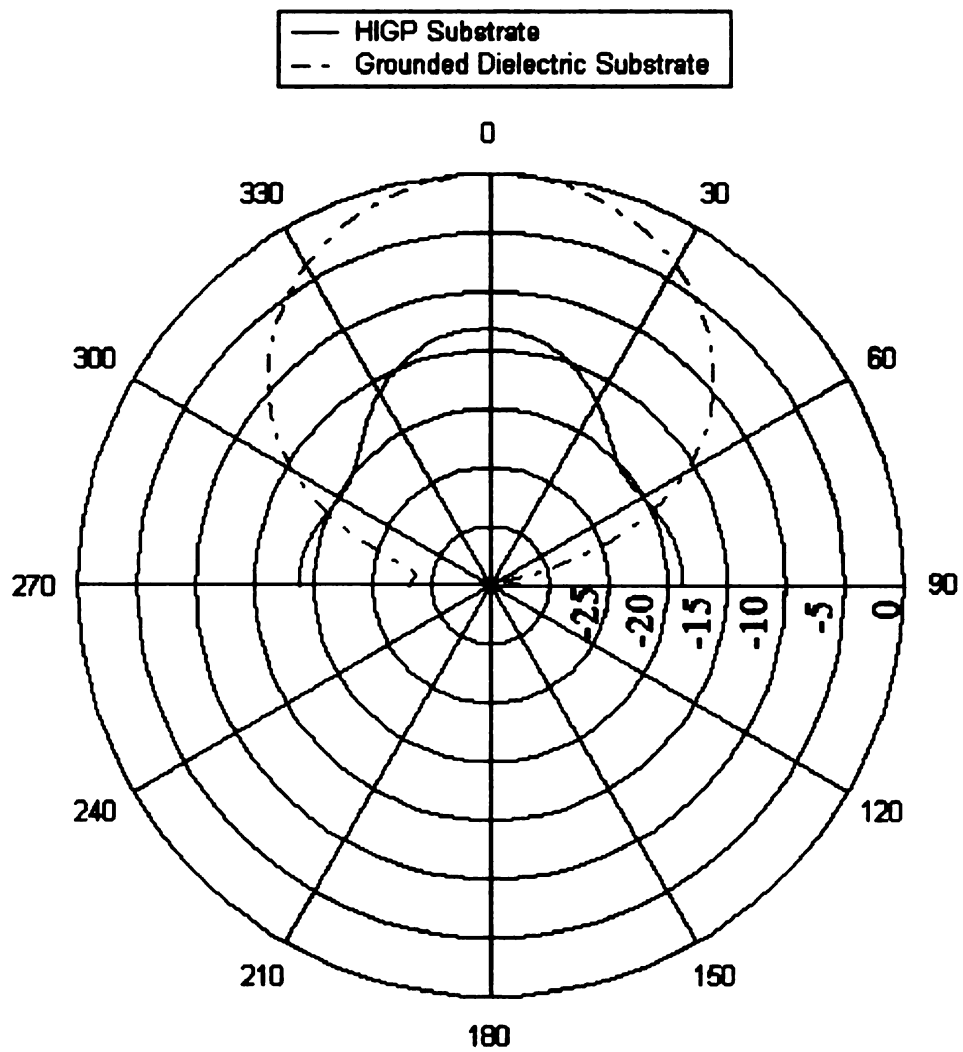
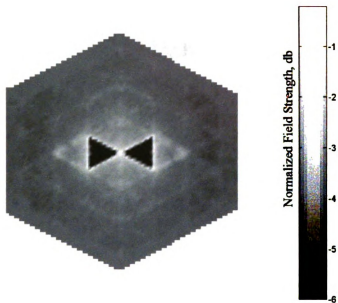
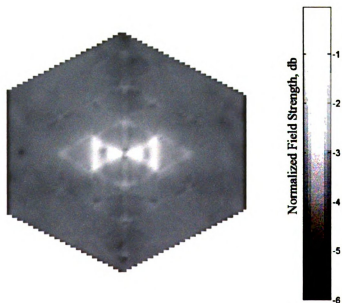


Figure 4-13: Broadside Normalized H-plane Pattern (gain, db) of the Bowtie Antenna with HIGP Substrate and Grounded Dielectric Substrate, F=5.58 GHz

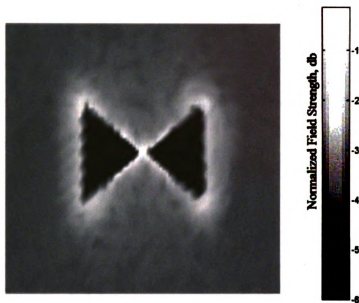


(a)

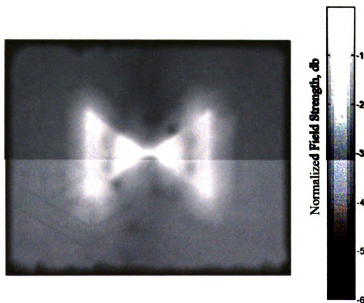


(b)

Figure 4-14: Normalized Tangential (a) and z-Directed E-fields for Antenna over HIGP Substrate



(a)



(b)

Figure 4-15: Normalized Tangential (a) and z-Directed E-fields for Antenna over Grounded Dielectric Substrate

4.5 Proposed Design not Computationally Tested

A final HIGP/antenna combination was designed at MSU, but was not computationally analyzed because of limitations in the program used to generate the FEM mesh of the structure. This design is shown in Figure 4-16.

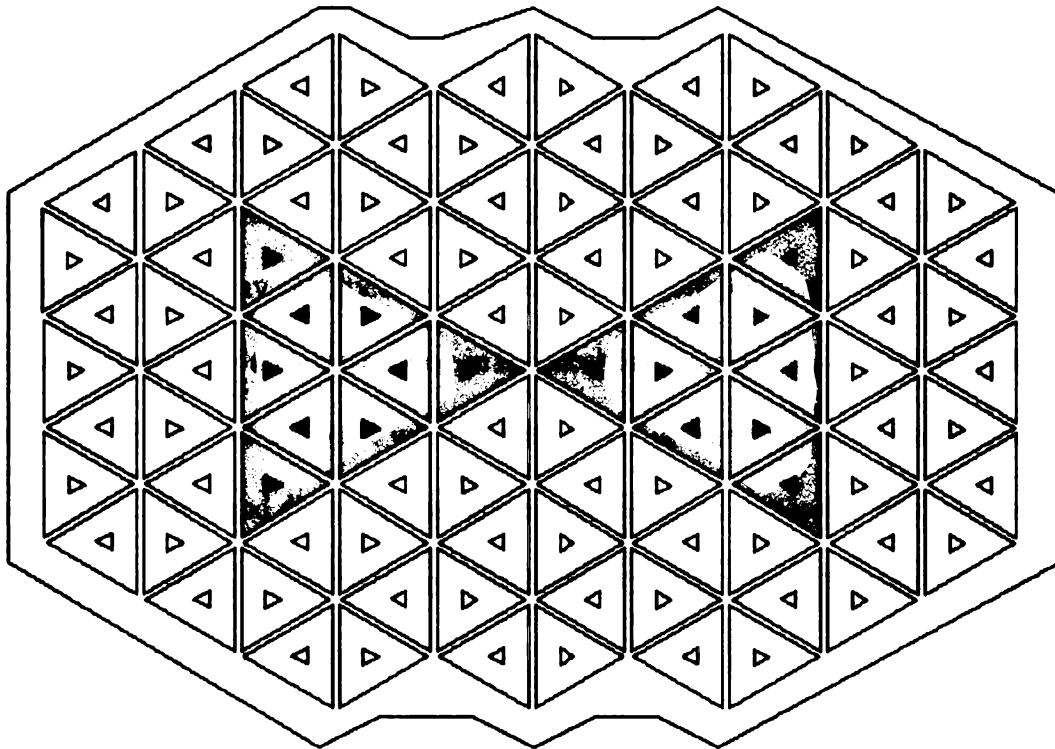


Figure 4-16: Untested Antenna/HIGP Four Layer Design

The shaded areas in the middle represent the two halves of the bowtie dipole on the top layer, continuous metal along with the dark triangles in the middle. The dielectric between the metal triangles is also specified as continuous metal in this region. The vertical prism edges for this layer are all dielectric, representing the dielectric substrate underneath. On the second layer, the antenna elements (gray triangles) as well as the other larger triangles are all specified as metal with vertical dielectric edges, representing the HIGP elements over top of dielectric substrate, and the dark smaller triangles, as well as all the other smaller triangles, are metal on the surface with metal vertical edges, representing vias. The antenna on the top layer is realized by creating a closed region in the meshing program that would enclose the antenna triangles and the dielectric in between (see Appendix A). This is a way of working around the constraint in the FEM code that all layers have identical cross-section, only different materials characteristics. However, because of an apparent bug in the meshing program, this structure could not be created in this fashion. *Skymesh* would not allow the creation of the region that encloses the HIGP elements and dielectric that make up the antenna on the top layer. Time would not allow for finding a new meshing program and tailoring the FEM code for reading in the output files generated by it.

This design would be the most optimized design thus far. The gap-width between HIGP elements is 0.5 mm, the HIGP element edge length is .84 cm, and the center-to-center spacing between vias is .54 cm. The HIGP is printed over a dielectric .762 cm (0.3") in thickness with a dielectric constant of 4.9, a thick version of FR4. The substrate separating the antenna from the HIGP layer is 59 mils in thickness, with a permittivity of 2.0. Each dipole half shown in Figure 4-16 is 2.3 cm in length. The resonant frequency of

the HIGP is 3.03 GHz, and the antenna is 118 electrical degrees at this frequency, from the input impedance plot of the bowtie dipole in Figure 4-3. Therefore, the antenna and the HIGP are now optimized together nearly perfectly. Furthermore, the guided wavelength at 3.03 GHz is 7 cm, making the ratio of HIGP elements-to-wavelength 13.2:1. The overall thickness of this design is .359" or .9 cm, slightly larger than $\lambda/8$. The distinct shape of the HIGP substrate is a product of removing as many HIGP elements as possible, thus streamlining the design and reducing unknowns. The border of the HIGP is only roughly 2.0 cm away from the low-frequency end of the antenna, or $\lambda/3.5$. Due to its low profile, small aperture area and high HIGP element periodicity, computational analysis should verify that this is the most streamlined yet operationally sound structure that could be designed with the proposed four-layer method.

CHAPTER 5

CONCLUSIONS AND GROUNDS FOR FUTURE WORK

This work has served several purposes. First, computational analysis of designs that have already been built and tested has been provided. Secondly, a new method of integrating dipole antennas with the ground plane that shields them from the backward half-space has been introduced, and in doing so, the commonly held notion that the periodicity of HIGP elements that form the substrate must be much smaller than the wavelength has been challenged. The four-layer design method allows for an electric-source antenna, with an electric field polarization vector parallel to the ground plane, to be placed near the ground plane ($> \lambda/4$) and still operate well. Decent, albeit not optimized performance is exhibited from these structures.

Several research questions exist for the structures presented here: first, can the input impedance of the dipoles be optimized simply by moving around the location of the probe feed. This would allow for better performance from the structures presented here without changing much about the structure itself. Second, computational analysis is needed of the final HIGP/antenna design from Section 4.5. This structure, based on the design equations and on the performance of less-optimized designs, could exhibit the best performance yet from a dipole antenna placed near a HIGP substrate. Finally, this thesis provides analysis of a wideband antenna with a single-band HIGP structure. It is possible that a HIGP design exists itself that operates in a wideband fashion. Such a structure would account for the different wavelengths that are radiated from a wideband antenna.

This substrate could be used in conjunction with simple spiral antennas or log-periodics to obtain good performance from surface mounted, low profile wideband antennas.

One of the hindrances to the design of HIGP/antenna structures using the finite element method is the enormous computation time required to accurately characterize the performance of the design. In this work, the antenna and HIGP substrate are always simulated together. It would be useful if the HIGP and antenna could be designed separately and then brought together in the final design, which would eliminate the time consuming process of 'tweaking' a design. It is suggested that the planar electromagnetic code *PMM* (Periodic Method of Moments) be used to determine the performance of the HIGP substrate. *PMM* simulates two dimensional infinite periodic surfaces, and has the capability of multiple-layer analysis, extending its usefulness to three dimensions. This code is generally used in the design of frequency selective surfaces (FSS) and radomes, in that the reflection from and transmission through the surface of plane waves at different frequencies and different polarizations can be analyzed. This code can be extended to HIGP substrates by examining the reflection phase of a plane wave at different frequencies from the surface. Furthermore, the design of dipole antennas by themselves is not easily done with the FEM code used in this work, in that this code assumes the antenna is surrounded by a cavity. Though good for patch antennas, the program is not easy to use for dipole and electric type antennas. It is suggested that a code that is conducive to printed dipoles be used here. The Numerical Electromagnetics Code (N.E.C.) would be a suitable means to this end. N.E.C. simulates wire antennas in free space. If enough wire elements are used, a continuous metallic triangle can be simulated. The resonant frequency of the antenna would then simply have to be scaled to

account for the dielectric substrate. Then, the FEM code *Prism* could be used to perform a high resolution frequency sweep of the final, optimized design of the antenna and HIGP together.

APPENDICES

APPENDIX A

CREATING INPUT FILES FOR PRISM

A.1 Methodology

One of the true challenges to this work was devising a way by which structures can be drawn in a standard drawing package, and then converted to the type of data that the FEM analysis program requires. The process by which a drawing becomes an input file to the Prism program is a lengthy one.

First, a model is drawn two-dimensionally in any CAD program. The one used for the structures presented here is called CadStd, and it is available on the Internet for free download. The structure is first drawn in discrete, closed sections using only polylines in CAD. For example, in the sample patch of Figure A-1 the outer square represents a dielectric border, and all space interior to that but exterior to the next rectangle is dielectric. The middle square represents the patch, and the smallest square represents the feed region.

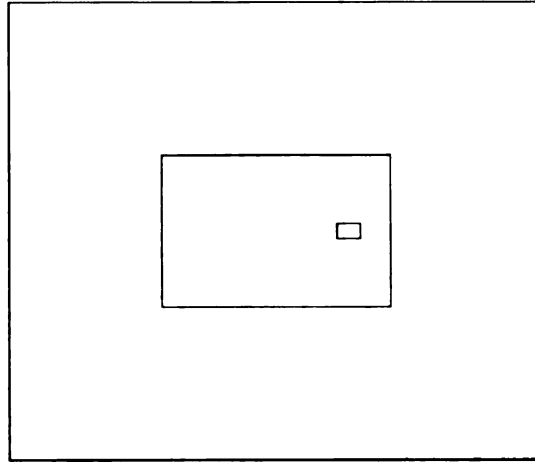


Figure A-1: Square Patch Drawn in CAD

All polylines are drawn counter-clockwise, a convention used by the meshing program, Skymesh. A counter-clockwise element is considered to be filled with some material, metal or dielectric, and a clockwise element is considered to be a hole. The CAD file is then exported to a DXF file, using the built in converter available with the package. A program called DXF2XYZ, also available for free on the Internet, is then used to convert the DXF file to an ordered set of points, with the vertices of each polygon grouped together and flagged uniquely. The result is a group of points that contains the start and stop point of each polyline drawn in CAD, representing the edges of each closed region. Edges from the same region are given a unique identifier (an incremented counter). A typical output file from DXF2XYZ is listed below, in Table A-1 , the second and third column are x and y values of the vertices of each line, and the first column is a unique identifier indicating that points with that same number belong to the same identifier. In this case, all points with the ID number 1 are vertices of the outer square, ID number 2 are vertices of the inner square, and ID 3 are vertices of the smallest, inner-most square.

1	0.0787	2.4409
1	0.0787	0.0787
1	2.8346	0.0787
1	2.8346	2.4409
1	0.0787	2.4409
2	0.8661	1.6535
2	0.8661	0.8661
2	2.0472	0.8661
2	2.0472	1.6535
2	0.8661	1.6535
3	1.8897	1.2992
3	1.7716	1.2992
3	1.7716	1.2204
3	1.8897	1.2204
3	1.8897	1.2992

Table A-1: Sample Output from DXF2XYZ

There are five points listed for the vertices of each square, yet a square has only four vertices. This is because when a polyline is drawn in CAD, the user must specify the start and stop points of each line. Therefore, the start vertex is listed twice, since the polyline goes around counterclockwise until it gets back to the start point. It is important to note that DXF2XYZ converts all dimensions to inches automatically. Then, the author wrote a Fortran code, called ReadXYZ, to read the output of DXF2XYZ and create the files necessary for SkyMesh to read. This program parses the output of DXF2XYZ for the unique identifiers and throws away the last point of each region, since nodes in Skymesh may only be listed once. It is recommended that each separate entity be drawn in a different layer in CadStd, because DXF2XYZ has the ability to parse out different layer from the DXF file and save them to different files. Since Skymesh relies on its input being listed from outermost entities to innermost, it is a good idea to draw similar entities

on different layers and use this feature of DXF2XYZ. An example of this would be something similar to Figure 4-1, where there are dielectric regions, metal pads, antennas and vias. The outer border would be drawn in one layer in CAD, the metal pads on a different layer, the vias on a third layer, the antenna elements on a fourth layer, and the two feed vias on a final layer. In DXF2XYZ, then, all these layers can be parsed out one at a time and saved to different files. The ReadXYZ program then takes these files and assembles them in a format acceptable to Skymesh.

The Skymesh program requires several different files in order to read in a geometry and create a mesh that has triangle edges of a user-defined length. These file include a .pts file, a .edg file, a .ref file, a .prj file, and a .geo file. The .pts file contains an ordered list of nodes (node number, x-coordinate, y-coordinate), as shown in Table A-2.

1	0.0787	2.4409
2	0.0787	0.0787
3	2.8346	0.0787
4	2.8346	2.4409
5	0.8661	1.6535
6	0.8661	0.8661
7	2.0472	0.8661
8	2.0472	1.6535
9	1.8897	1.2992
10	1.7716	1.2992
11	1.7716	1.2204
12	1.8897	1.2204

Table A-2: Sample Skymesh .pts File

These nodes contain the vertices of the squares/polylines that make up the closed regions of Figure A-1. Note that the .pts file does not contain the extraneous endpoint that was found in the .xyz file. The .edg file, listed in Table A-3, contains an ordered list of edges that specify which nodes in the .pts file are connected together to make an edge (edge number, node 1, node 2).

```

@normal    0 0 1
  1         1     2
  2         2     3
  3         3     4
  4         4     1

@normal    0 0 1
  5         5     6
  6         6     7
  7         7     8
  8         8     5

@normal    0 0 1
  9         9    10
 10        10    11
 11        11    12
 12        12     9

```

Table A-3: Sample Skymesh .edg File

This says that edge 1 connects nodes 1 and 2, edge 2 connects nodes 2 and 3, and so on. The '@normal 0 0 1' line defines coefficients of a three-dimensional rectangular-coordinate unit vector that is normal to the drawing: $0\hat{x} + 0\hat{y} + 1\hat{z}$, which means that the drawing lies purely in the x-y plane. There are three sections of edges, corresponding to three closed regions in the drawing.

The .ref file in Skymesh specifies the maximum edge length for any element. In this case, the edge length corresponds to the length of the edge of each triangle. A standard practice is to always use edge lengths that are $\lambda/15$ - $\lambda/20$ at the highest frequency. Coarser meshing can cause incorrect field values to be calculated on the surface of the mesh. An example of a .ref file is found in Table A-4. The word g-face specifies that the following data corresponds to a closed region. The regions are in the same order as they are found in the .pts file, so g_face 1 corresponds to the dielectric region of the square

patch of Figure A-1, g_face 2 corresponds to the metal patch, and g_face three corresponds to the feed region. The first number is the normal edge length (which has no meaning in a two-dimensional surface mesh!) and the second number is the tangential edge length, the important one in this case.

auto		
g_face		
1	0.12	0.12
g_face		
2	0.12	0.12
g_face		
3	0.02	0.02

Table A-4: Sample Skymesh .ref File

The .prj file simply specifies in what files to look for all of this information and where to store the resulting output. The data in this file is similar to that of Table A-5.

# Project File	F:\square\Patch_only\patchOnly.prj - Saved on 6-Jun-02 at 21:12
GEOMETRY	Patchonly.geo
REFINEMENTS	patchOnly.ref
DENSITY	Patchonly.den
MESH	Patchonly.fem
GRID	Patchonly.grd

Table A-5: Sample Skymesh .prj File

The geometry file specifies where to find the points (.pts file) and the edges (.edg file), and its contains only the following line:

```
@2d_style "Patchonly.pts" "Patchonly.edg"
```

where @2d_style specifies a two-dimensional drawing. The refinements file, as discussed above, contains information about the maximum edge lengths. The DENSITY, MESH AND GRID files are all outputs of Skymesh. The particular format of these files is immaterial, but it is important to note that prism uses the GRID file (.grd) as its input.

The program ReadXYZ must be modified every time a new antenna is drawn to ensure that the outer regions are input into the Skymesh files in the correct order. This information is specified in the .pts, .edg, and .ref files, where the nodes, edges and edge lengths of the outer regions are specified first, and then any inner regions are specified. This is made easy by drawing regions in CAD in different layers, and then parsing out each individual layer in DXF2XYZ and saving it in a separate file. ReadXYZ then reads the files specified (in order from outer to inner) by the user. The code that is found in the next section is that which was used to generate the mesh of Figure 4-1. The subroutine getPts actually writes the data to the file. This subroutine is first called for the outer border, then the HIGP metallic pads, and then the vias that lie inside the pad. Then the code is called for the antenna (the two middle triangles in the figure) and the for the feed regions for those triangles. These were drawn separately so that a different edge length could be specified for these two regions. The details of other Prism input files are immaterial, but a good grasp of the .grd process is vital to creating accurate meshes. This entire process is summarized in Table A-6.

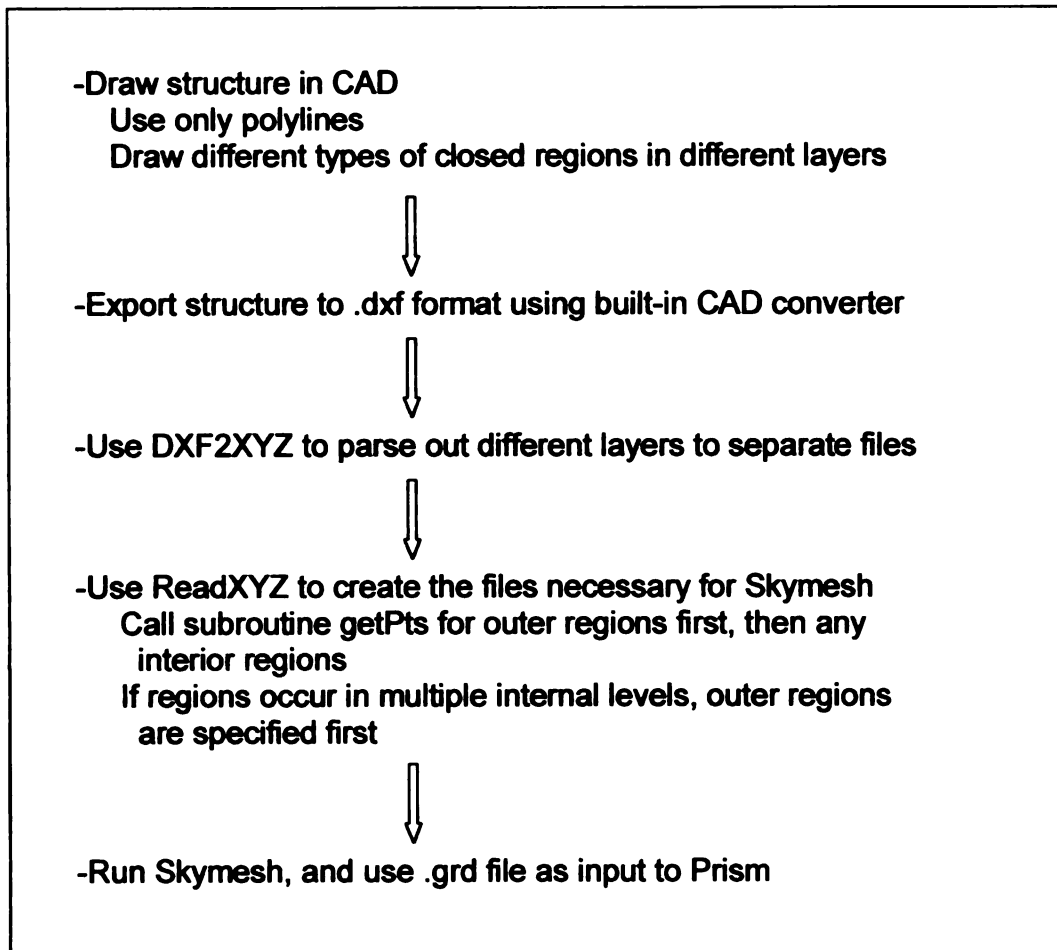


Table A-6: Flowchart for Creating the Prism Input Files

A.2 ReadXYZ Fortran Code for Reading DXF2XYZ Ouput

```
c*****
***** Order of Skymesh input file creation:
*****      1. Create drawing in CAD (.cad file)
*****      2. Export .cad file to .dxf file using 'Export'
*****          option in CAD program
*****      3. Use DXF2XYZ.exe program to convert .dxf file
*****          to x,y,z, triplet
*****      4. This program converts .xyz file to .pts and
*****          edg files used by Skymesh

program readXYZ
use dfport
implicit none

character*70 directory,infile,the_date
integer totPts,totSecs,totEdges
real*8 edgeSize

infile='bow_higp'
directory='f:\bowtie\bow_higp\'

open(unit=12,file=trim(directory)//trim(infile)//'_outerBo
+rder.xyz',status='old')

open(unit=13,file=trim(directory)//trim(infile)//'_element
+s.xyz',status='old')

open(unit=14,file=trim(directory)//trim(infile)//'_vias.xy
+z',status='old')

open(unit=15,file=trim(directory)//trim(infile)//'_antenna
+.xyz',status='old')

open(unit=16,file=trim(directory)//trim(infile)//'_feed.xy
+z',status='old')
```

```
open(unit=7,file=trim(directory)//trim(infile)//'.pts',sta
+tus='unknown')
```

```
open(unit=8,file=trim(directory)//trim(infile)//'.edg',sta
+tus='unknown')
```

```
open(unit=9,file=trim(directory)//trim(infile)//'.ref',sta
+tus='unknown')
```

```
open(unit=10,file=trim(directory)//trim(infile)//'.prj',st
+atus='unknown')
```

```
open(unit=11,file=trim(directory)//trim(infile)//'.geo',st
+atus='unknown')
```

```
1  format(a,2x,a)
   write(9,(''auto''))

   call fdate(the_date)
   write(10,'(a,a,a,a)') '# Project file - ',trim(infile)
+, '.prj,Modified on ',trim(the_date)
   write(10,1) 'GEOMETRY',trim(infile)//'.geo'
   write(10,1) 'REFINEMENTS',trim(infile)//'.ref'
   write(10,1) 'DENSITY',trim(infile)//'.den'
   write(10,1) 'MESH',trim(infile)//'.fem'
   write(10,1) 'GRID',trim(infile)//'.grd'
2  format('@2d_style "',a,'" ',2x,'" ',a,'" ')
   write(11,2) trim(infile)//'.pts',trim(infile)//'.edg'

   totEdges=0
   totPts=0
   totSecs=0
   edgeSize=0.105
   call getPts(totPts,totSecs,totEdges,edgeSize,12)

   edgeSize=0.157
   call getPts(totPts,totSecs,totEdges,edgeSize,13)

   edgeSize=.08
   call getPts(totPts,totSecs,totEdges,edgeSize,14)
```



```

        edgeSize=1.0
        call getPts(totPts,totSecs,totEdges,edgeSize,15)

        edgeSize=.03
        call getPts(totPts,totSecs,totEdges,edgeSize,16)
    end
C*****
*
C*****THIS SUBROUTINE PERFORMS THE ACTUAL DATA PARSING
      subroutine getPts(totPts,totSecs,totEdges,edgeSize,
+file_read)
      implicit none

      integer totPts,totSecs,totEdges
      integer
marker(1000),i,j,ioerr,numPts,start_edg,stop_edg
      integer secLoc(100),ptsPerSec(100),numRegions
      integer file_read,region
      real*8 xTemp(1000),yTemp(1000),edgeSize

      region=totSecs
      numPts=0
      numRegions=1
      totSecs=totSecs+1
      marker=0
      ioerr=0

      do while(ioerr .eq. 0)
          numPts=numPts+1
          read(file_read,*,iostat=ioerr)marker(numPts),
+xTemp(numPts),yTemp(numPts)
      enddo
      numPts=numPts-1

C*****FIND LOCATIONS OF DIFFERENT CLOSED REGIONS IN THE
XYZ C*****FILE,BASED ON IDENTIFIER FLAG IN DXF2XYZ
      secLoc(1)=1
      do i=1,numPts-1
          if(marker(i) .ne. marker (i+1)) then
              ptsPerSec(numRegions)=i-secLoc(numRegions)
              totSecs=totSecs+1
              numRegions=numRegions+1
              secLoc(numRegions)=i+1
          endif
      enddo

```

```

        enddo
        ptsPerSec(numRegions)=numPts-secLoc(numRegions)

        do i=1,numRegions
            do j=secLoc(i),secLoc(i)+ptsPerSec(i)-1
                totPts=totPts+1
                write(7,15) totPts,xTemp(j),yTemp(j)
            enddo
            write(7,*)

            start_edg=totEdges+1
            stop_edg=totEdges+ptsPerSec(i)
            write(8,25)
            do j=start_edg,stop_edg-1
                totEdges=totEdges+1
                write(8,20) j,j,j+1
            enddo
            totEdges=totEdges+1
            write(8,20) j,j,start_edg
            write(8,*)
            write(9,30) region+i,edgeSize,edgeSize
        enddo

15  format(2x,I4,4x,F12.6,4x,F12.6)
20  format(2x,I4,4x,I4,4x,I4)
25  format(2x,'@normal 0 0 1')
30  format(2x,'g_face',/,6x,I3,5x,F6.3,F6.3)
    return
end

```

REFERENCES

-
- [1] R.S. Elliott, "Antenna Theory and Design," Prentice Hall, New Jersey, 1982, pp. 27-38
- [2] E. Yablonovitch, T.J. Gmitter, "Photonic band structure: the face-centered-cubic case," *J. Opt. Soc. Am. A*, vol. 7, no. 9, Sep. 1990
- [3] D.F. Sievenpiper, *High-Impedance Electromagnetic Surfaces*, Ph.D. dissertation, University of California at Los Angeles, Los Angeles, CA, 1999
- [4] K.J. Golla, *Broadband Applications of High Impedance Ground Planes*, M.S. Thesis, Air Force Institute of Technology, Dayton, OH, March 2001
- [5] L.C. Kempel, "Anisotropic Right Prism Finite Element-Boundary Integral Theory," unpublished, April 2002
- [6] C.A. Balanis, "Antenna Theory," 2nd Ed., John Wiley and Sons, 1996
- [7] E.R. Brown, C.D. Parker, E. Yablonovitch, "Radiation properties of a planar antenna on a photonic-crystal substrate," *J. Opt. Soc. Am. B*, vol. 10, no. 2, Feb. 1993
- [8] S.D. Cheng et al, "Optimized dipole antennas on photonic band gap crystals," *Appl. Phys. Lett.*, vol 67, no. 23, Dec. 1995
- [9] M. Thévenot, C. Cheype, A. Reineix, B. Jecko, "Directive Photonic-Bandgap Antennas," *IEEE Trans. Microwave Theory Tech.*, vol. 47. no. 11, Nov. 1999
- [10] R. Coccioli et al, "Aperture-Coupled Patch Antenna on a UC-PBG Substrate," *IEEE Trans. Microwave Theory Tech.*, vol. 47, no. 11, Nov. 1999
- [11] R. Gonzalo, P. de Maagt, M. Sorolla, "Enhanced Patch-Antenna Performance by Suppressing Surface Waves Using Photonic-Bandgap Substrates," *IEEE Trans. Microwave Theory Tech.*, vol. 47, no. 11, Nov. 1999

-
- [12] L. Hunt, "Analysis of Microstrip Antennas on Substrates with High Permeability," M.S. Thesis, Michigan State University, East Lansing, MI 2002
- [13] G.H. Brown, O.M. Woodward, "Experimentally Determined Radiation Characteristics of Conical and Triangular Antennas," *RCA Rev.*, Dec. 1952

MICHIGAN STATE UNIVERSITY LIBRARIES



3 1293 02356 3756